Title
Characterization of varnish removal in differing environmental conditions

Author
Ades, Mickeal T

Publication Date
2019

Peer reviewed|Thesis/dissertation

UNIVERSITY OF CALIFORNIA, MERCED

Characterization of varnish removal in differing environmental conditions

by

Mickeal T. Ades

A Thesis submitted in partial satisfaction of the

requirements for the degree of

Master's

in

Mechanical Engineering

Committee:

Professor Ashlie Martini, Advisor

Po-Ya Abel Chuang

Gerardo C. Diaz

The Thesis of Mickeal Ades is approved:

_____

Ashlie Martini, Adviser Date

_____

Po-Ya Abel Chuang Date

_____

Gerardo C. Diaz Date

University of California, Merced

Table of Contents

Table of Figures/ Tables

Acknowledgments

I would like to give a heartfelt thank you to Professor Martini, for giving me the opportunity to work on this project, your mentorship and guidance have been invaluable. To the engineering faculty of University of California Merced for giving me the tools and confidence to work on complex engineering problems. To Mandy, Monique and Ilexia for your love, patience and support. Finally, to Terry you nearly lost all, and forever changed my prospective on life.

Abstract

Varnish is an oxidative byproduct of lubrication that builds up on mechanical components during operation. Varnish must be removed to enable optimal performance of a mechanical system. Many mechanical systems reach very high temperatures; for example, gas turbine engines have areas of extreme temperature up to the 2000˚C. This means that oxidation and oxidative byproducts are a constant issue in these systems. There are many ways to mitigate varnish buildup and control oxidative byproducts, but chemical flushes are necessary if the varnish buildup reaches a critical point. This research investigated the effectiveness of different formulations of chemical cleaners in a standardized low flow test and characterized the effects of flow rate, temperature and concentration for one of those cleaners. The comparative cleaner tests showed that many commercial cleaners did not remove substantial varnish at 0.5 GPM and 90° C. Only two fluids were capable of removing significant varnish during the 50-hour test. One of those fluids was then tested over a range of temperatures, flow rates and cleaner concentrations. The temperature tests revealed that removal rate increases with increasing temperature. The effect of temperature was described by a polynomial trend that suggested an effective operating temperature range for varnish removal. The concentration of chemical cleaner additives had a large effect on the removal rate, with low concentrations removing very little varnish even after extended periods of time. This effect was governed by a power law relationship with diminishing returns at the higher concentrations. Flow rate tests showed a distinct trend of removal rate increase with flow rate increase. The relationship between varnish removal and flow rate was described by a power law where the effect of increasing flow rate diminished at higher flow rates. Flow rate also affected the size and distribution of varnish particles collected on a downstream filter and the results showed that the filter size needed for optimal varnish removal should be flow rate dependent. The effect of flow rate was further analyzed using computational fluid dynamics models. The simulations showed that increasing flow rates cause higher shear stress at the surface of the varnish, facilitating varnish removal. Simulations also showed that geometric features on the varnish can affect shear rates and in turn the rate of local varnish removal. Overall, this study showed the importance of operating conditions and their impact on varnish removal and provided information that can help in the formulation of new cleaners as well as selection of operating conditions and filter media for the most efficient varnish removal.

1 Introduction

1.1 Lubricants

Any substance used to minimize friction and wear between moving parts can be called a lubricant. These lubricants are primarily used to increase efficiency and lifetime of mechanical systems. Many different forms of lubricants are used and can generally be categorized as solid, liquid, or gaseous. Solid or dry lubricants are used on their own in applications or can be used in combination with liquid lubricants to improve wear and friction protection[1]. Gaseous lubricants have a very low viscosity and are primarily used in a high-pressure form such as compressed air. Each mechanical system requires the selection of an appropriate lubricant. There are over 10,000 different forms and types of lubricants used around the world [2]. In this work we will solely focus on liquid lubricants.

A liquid lubricant is a fluid introduced between moving parts to create a viscous layer that separates the moving surfaces, minimizing wear and friction. Liquid lubricants also perform many secondary functions in a mechanical system. For example, the steady flow of oil can remove heat and wear particles from the system[3]. Selection of the correct liquid lubricant for a mechanical system can dramatically increase the efficiency of that system. Liquid lubricants were originally made of fats and natural oils derived from plant- and animal-based raw materials. Lubrication markets changed dramatically in 1859 after the first oil well was drilled, changing the supply and quality of liquid lubricants[4]. Lubricants have evolved from mineral oils to many different blends of petrochemically modified synthetic oils. Each of these blends have been formulated to increase the lubrication properties over a wide range of environmental conditions [5].

The majority of liquid lubricants are formulated from petroleum-based products or crude oil [6]. Crude oil is made up of complex hydrocarbon molecules. To separate crude oil into its functional parts, it is subjected to distilling and other refining processes. This separates crude into base oil, paraffin, asphalt and various grades of fuel. During the distillation process, hydrocarbon chains are evaporated and separated by size. Base oil, which makes up 90% of most lubricants, has a carbon backbone between 16 to 70 carbon atoms long [2]. Aromatics and wax are removed in later refinement steps. The hydrocarbon chain can be further refined to fit certain applications.

When a lubricant degrades during operation, it can form varnish and sludge. The conditions under which a lubricant will degrade, and the corresponding varnish or sludge formation, are directly related to the lubricant's viscosity and its composition. These two topics are reviewed next.

1.2 Viscosity

Viscosity is the measurement of a fluid's resistance to flow. An easy example is the difference between the flow of molasses and the flow of water. A lubricant's viscosity changes with multiple factors, including temperature, shear rate, and pressure [7]. A lubricant's effectiveness

is correlated to its viscosity which dictates its film strength or ability to separate moving parts. The importance of viscosity to a lubricant's effectiveness is vital. A system that is operating at low temperature and small loads will need a lower viscosity lubricant than a system that is working at high temperature and high loads.

Viscosity index is a measurement of the rate of change of viscosity due to the change in temperature of the fluid, as shown in Figure 1-1. The higher the viscosity index of a lubricant, the less its viscosity will change with changes in temperature. This is a great advantage for synthetic oils which have a more consistent molecular weight and behave in a much more predictable fashion. The viscosity index, in many ways, is the most important classification of a lubricant[8]. In complex machinery, pressures and temperatures fluctuate drastically due to surface phenomena [9]. A high viscosity index can ensure that the lubrication works consistently throughout the mechanism.

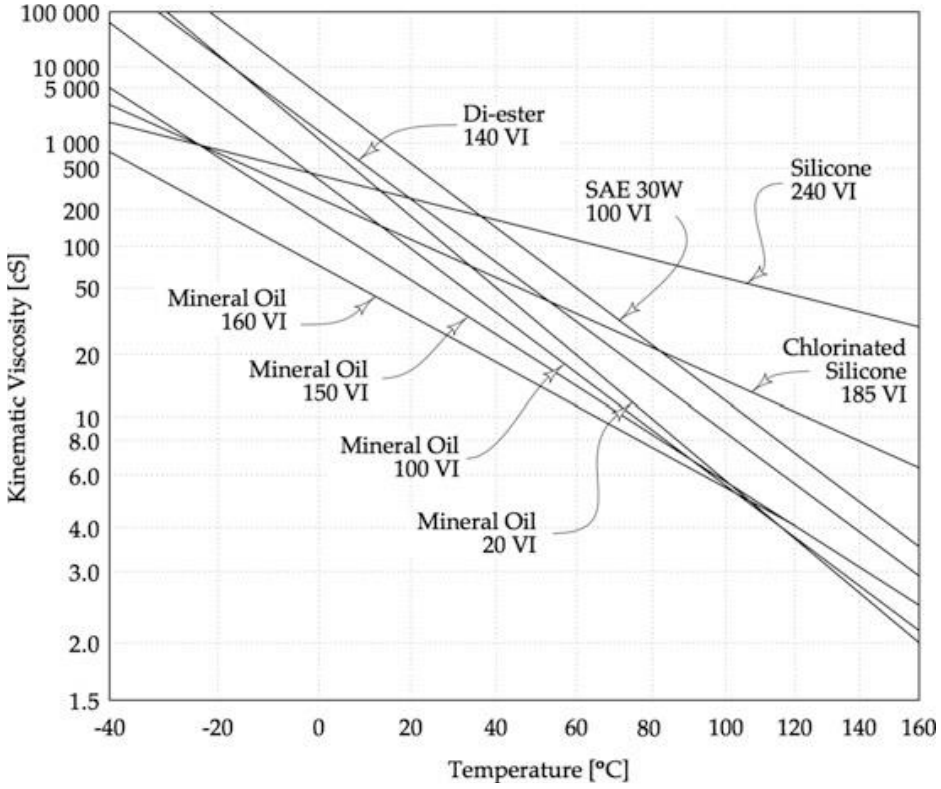

Figure 1-1: Kinematic viscosity vs. temperature (° C) of several common oils. The viscosity index is correlated to the slope of the line or the rate of change in the viscosity due to temperature change [10].

Viscosity is normally measured in pressure per second, and this measurement is called dynamic viscosity. Dynamic viscosity is best explained by considering two parallel surfaces separated by a layer of fluid having a measured thickness. A force is needed to move the top surface parallel to the bottom surface *F*. The magnitude of this force is dependent on the area of the plate in contact with the fluid *A*, the relative speed of the surfaces *u*, and the thickness of the fluid film separating the plates *h* [11].

$$F \propto A * \frac{u}{h} \quad (1\text{-}1)$$

The viscosity indicates the resistance to flow and allows us to calculate the force needed to move the plate at a given speed (*u*) and gap (*h*).

$$F = \frac{\eta A u}{h} \quad (1\text{-}2)$$

Solving for viscosity then gives:

$$\eta = \tau * \frac{u}{h} \quad (1\text{-}3)$$

Where η is the dynamic viscosity, τ is the shear stress and u/h is the shear rate. In international units, viscosity is normally measured in centipoise (cP). The SI unit for dynamic viscosity is Pascal second. The relationship between centi-Poise and Pascal-second is 100 (cP) 0.1 (Pa*s)[11]. Dynamic viscosity is the ratio between shear stress and shear rate. Kinematic viscosity (v) is a ratio of the dynamic viscosity to the density ρ at a specific temperature and pressure.

$$v = \frac{\eta}{\rho} \quad (1\text{-}4)$$

1.3 Additives

Additives are chemicals included in a lubricant formulation to perform specific functions. Additives are classified based on their influence on a lubricant's behavior. This separates additives into two main categories, surface and bulk additives. Surface additives modify the physicochemical properties of the metal surfaces affecting friction, corrosion, and wear. The bulk additives influence the physical and chemical properties of the fluid, such as the viscosity-temperature characteristics, dispersive properties and oxidative stability [11].

Due to the compatibility or incompatibility of additives, they are normally formulated for a specific function. A good additive package can increase the lubrication properties of the base oil, but functional mismatch can lead to large-scale degradation and deposit formation. Additives make up a small portion of the lubricant; nevertheless, the lubricating properties are primarily due to the additives. A good additive package improves not only the performance of the lubricant, but the life of the oil [7].

When two metal surfaces are in contact, hydrodynamic lubrication does not occur at the point of initial movement. At this initial point, which occurs during starting and stopping, a lubricant must operate in a boundary or mixed lubrication regime to reduce friction and wear [12]. Chemical additives that serve this function fall into three major groups: boundary, antiwear, and extreme pressure. Boundary additives are usually larger molecules like fatty acids that can reduce asperity contact. At the micro scale, all surfaces are rough, and large fatty acid molecules maintain the lubrication layer between rough surfaces. Antiwear additives improve the

hydrodynamic lubrication properties at normal working temperatures and pressures. Lastly, extreme pressure additives work outside of the normal temperature and pressure regimes.

When opposing surfaces are moving at a sufficient velocity, hydrodynamic lubrication occurs. In this regime a thin film of lubricant separates metal surfaces preventing wear. Consistent flow properties are important to maintain mechanical continuity at different output loads. Chemical additives that maintain the bulk fluid properties assist in this consistency. These additives are represented by antioxidants, dispersants and viscosity improvers. Antioxidants additives neutralize free radicals and reduce the effect of oxidation[3]. Dispersants assist in maintaining homogeneity of the lubricant when foreign bodies are introduced. Viscosity improvers reduce the viscosity temperature dependency for more consistent viscosity through all working temperatures.

1.3.1 Boundary

Friction modifiers, also known as boundary additives, are generally formed from fatty acids with a polar carboxyl group (-OH) at one end. This long-tailed molecule reacts with the surface creating a monolayer of lubricant that is effective at low temperatures and pressures. Boundary layer absorption reduces friction by creating a low shear film on the surface and reducing asperity contact between surfaces. These molecules are made of an unbranched chain of carbon atoms that must be long enough to ensure that a stable close packed monolayer is formed. In general, boundary layer additives consist of a ~18 unsaturated carbon backbone that can be manipulated to assist in anti-corrosion properties [7]. The working temperature of the carboxyl group adherence is much lower than temperatures in many operating vehicles and the boundary layer tends to desorb from the surface at higher temperatures rendering it ineffective.

1.3.2 Antiwear

Antiwear additives are molecules that absorb to the metal surface of parts. These reactions form a tribochemical film or layer that is much more stable and durable than a monolayer. This multilayer is most effective at general operating pressures and temperatures. Antiwear additives make up 1 to 3% by weight of a lubricant mixture and are often formulated from phosphorus compounds [11]. Direct reactions with the surface are integral to the success of antiwear additives, so good compatibility between the surface (which is usually ferrous) and the additive is necessary.

1.3.3 Extreme pressure

Extreme pressure additives react with metal surfaces under extreme conditions, where the pressure and temperature are well above normal operating parameters. These molecules form a layer on the metal surface by physisorption or chemisorption. Extreme pressure additives contain nonmetals such as sulfur, antimony, iodine, or chlorine molecules [5]. Under conditions where hydrodynamic lubrication is not feasible, surface lubrication reduces friction and heat. Extreme pressure additives primarily react with the surface only at high temperatures and are inactive under normal working conditions. Extreme pressure additives react strongly with the

surface inducing a corrosion layer at the metal surface. The concentration of this type of additive is usually kept to a minimum to reduce corrosion in the system.

1.3.4 Antioxidants

Antioxidants reduce the percentage of free radicals in the system. Many lubricant formulations contain antioxidants to prolong the working life of the oil. Lubricants can contain naturally occurring antioxidants such as nitrogen or sulfur compounds, as shown in Figure 1-2.

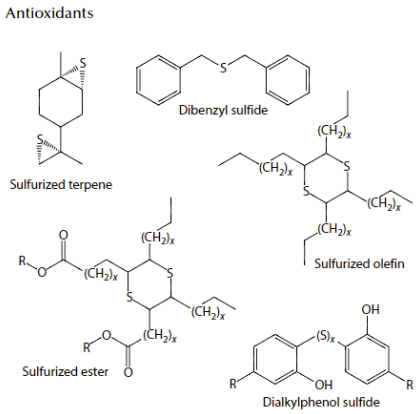

Figure 1-2: Example of sulfur containing antioxidants. R represents a reactive species that can seek out free radicals[13]

In addition to naturally occurring antioxidants, zinc dialkyldithiophosphate, phenol derivatives, organic phosphate, amines and metal derivatives are often added to a formulation [11]. The primary antioxidant function is to scavenge the lubricant for free radicals.

1.3.5 Dispersants

For a lubricant to have consistent properties, the fluid must remain homogeneous even when exposed to contaminants or phase change. In operation, lubricants are exposed to many byproducts of the system's function, such as combustion products, contaminants, and fluid leaks. The contaminants affect the lubricity of lubricant and can render it ineffective[14]. One mechanism of this degradation is when varnish precursors agglomerate into larger particles, where contaminants group and clog filters and channels. Detergents and dispersants are materials that chemically react with oxidation and wear products and assist in suspending them in the fluid. The suspended particles can be removed through a filtration system, preventing accumulation [5].

Detergents and dispersant additives are normally formed from a molecule having a polar hydrophilic head. This polar hydrophilic head is attracted to the contaminants in the lubricant while an oleophilic tail prevents adherence to the metal surface and agglomeration. They tend to adsorb on foreign particle surfaces, forming an aggregate of molecules that separates the oil from the foreign body. A stable isotropic liquid mixture results from this process. Calcium carbonate is a common additive that assists in the formation of micelles to the detergent. The

detergent is instrumental in allowing a lubricant to operate in the working environment, or if oxidation occurs. There are many classes of detergents: metal sulfonates, metal phenates, metal salicylates, and metal phosphonates and thiophosphonates [7]. These additives prolong the life expectancy of the lubricant and assist in the resistance of degradation.

1.3.6 Viscosity Improvers

Lubricants are designed to maintain a viscosity range throughout the working temperature of an engine. Viscosity improving additives reduce the effect of temperature on viscosity allowing for a larger working temperature range. These additives are usually high molecular weight polymers which are dissolved in the lubricant [15]. The larger the molecular weight, the more difficult it is for the polymer to dissolve in the base lubricant and solubility, like viscosity, is highly dependent on temperature [1]. At low temperatures, viscosity improvers are coiled tightly into small dense particles. As the temperature increases, these molecules unwind giving additive viscosity benefits at the higher temperatures. This concept is illustrated in Figure 1-3. A viscosity improver will increase the viscosity index of a given lubricant.

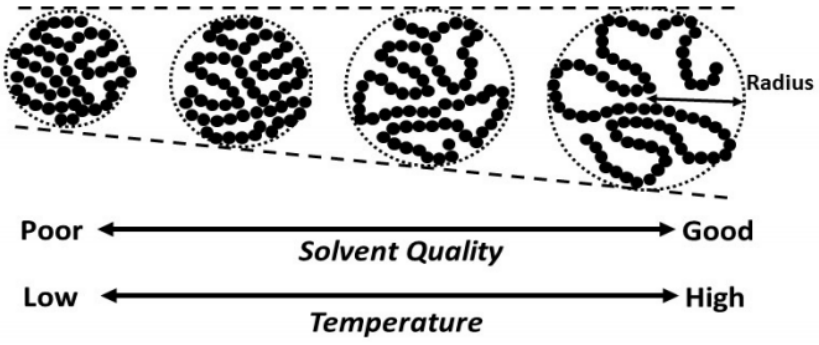

Figure 1-3: The effect of temperature on polymeric viscosity improver additives. The solvent or oil remains constant, so at low temperature these large molecules are coiled and have minimal effect on viscosity, yet at high temperature they expand and increase the viscosity of the overall fluid [16].

1.4 Varnish

Varnish is a polar molecule that builds up on metal engine parts, or wetted surfaces in a turbine lubrication system. The buildup can affect any moving mechanical part, but the primary adverse effects occur in areas of low tolerances such as servos and control valves that may begin to stick [17]. Valves have a susceptibility to varnish accumulation due to their low tolerances.

1.4.1 Varnish Composition and Properties

Varnish is primarily made up of repeating units called monomers. As these monomers bond to each other, they form longer and longer chains which will increase the strength of the chains [2]. The polymer solution is made up of many individual polymer chains that are bonded covalently through the backbone and by covalent, hydrogen, and van der Waals bonds from chain to chain.

These cross-linking bonds give additional strength the polymer[18]. The molecular weight of a polymer is in part an average of the length of all the individual polymer chains [19]. The larger the molecular weight, the more likely a polymer is to become entangled. This entanglement allows for more cross-linking bonds that strengthen the polymer [20]. A critical molecular weight is the point at which entanglement occurs increasing mechanical strength [18]. Equation 1-5 shows the molecular weight where *N* is the number of i^{th} monomers and *M* is the mass of the i^{th} molecule. Equation 1-6 gives the relationship between a polymer strength σ and its molecular weight, where *A* and *B* are constants specific to the polymer.

$$\bar{M} = \sum_i \frac{N_i M_i}{N_i} \quad (1\text{-}5)$$

$$\sigma = A - \frac{B}{\bar{M}} \quad (1\text{-}6)$$

Temperature has a large influence on a polymer's mechanical strength [21]. Cross-linked bonds can be influenced by temperature, but the primary effect of temperature on the polymer strength is in the degrees of freedom of the chains. As temperature increases in amorphous portions of the varnish, the confirmation can randomize, which negates chain-to-chain bonds [22]. In the crystalline regions of the polymer chain, folded surfaces become flexible and allow for lateral slipping that can result in lower density and, therefore lower strength of the overall polymer, as shown in Figure 1-4.

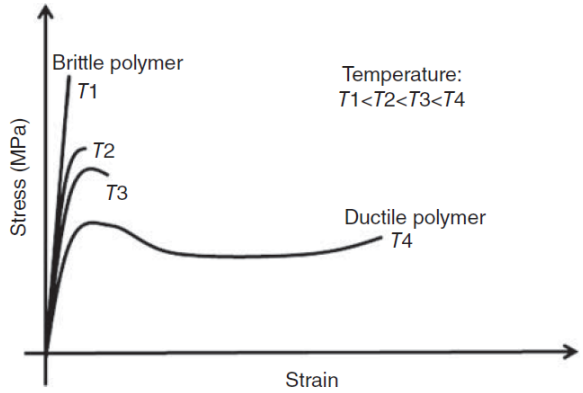

Figure 1-4: The effect of temperature on polymer strength [23].

The temperature at which a polymer exhibits a consistent stiffness or Young's modulus is called the glass transition temperature (T_g). The glass transition temperature can vary greatly from the melting temperature of the polymer. This means that a polymer can exhibit multiple states of mechanical properties between its transition to crystallinity (T_m) and its glass transition (T_g). A polymer can have many stages, starting with its transition from a liquid to a crystalline material. This is called a first order transition, illustrated in Figure 1-5. The polymer can continue to solidify from and will pass through numerous second order transitions from a rubbery state to a glassy state in which the mechanical strength of the polymer will change.

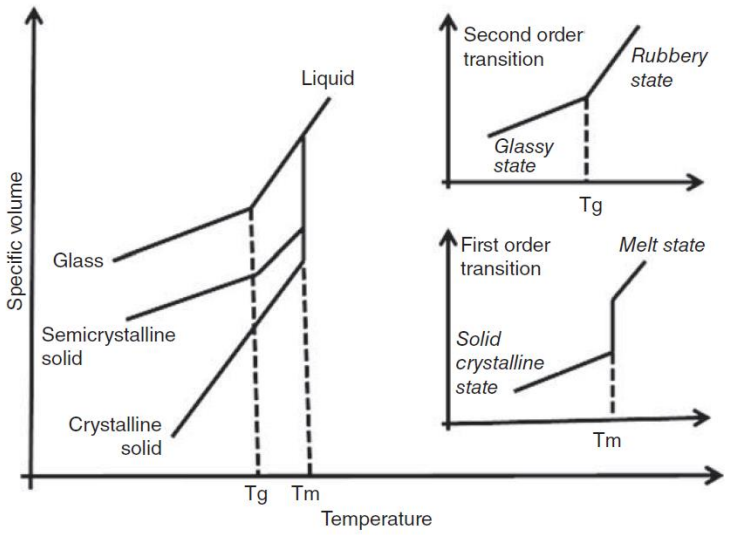

Figure 1-5: The possible glass transition pathway of a polymer as it is cooled from liquid. Upper subplot shows a second order transition from a robbery state to a glass state. Lower subplot shows a first order transition from liquid to crystalline material [23].

Polymer degradation occurs when the chemical structure, physical property, and appearance change. This may be a result of chemical cleaving or scission of the backbone of the polymer chain [24]. There are many types of polymer degradation, photo oxidative, thermal oxidative, ozone induced, and mechanochemical [25]. We will focus on mechanochemical degradation in which three primary steps occur. First the polymer is exposed to a solvent, which changes the structure of the backbone chain. Second, the molecular weight is reduced by scission of random covalent bonds. In the third step, the polymer can be dissolved into smaller and smaller units or reorganized [3]. Polymer degradation primarily results from a reduction in the mean length of the polymer chains and loss of density which diminishes the strength of the polymer. This reduction in strength allows for dissolution of degraded particles into a solvent.

1.4.2 Varnish Formation

Varnish is a byproduct of the degradation of the hydrocarbon-based fluid of a lubricant. Degradation occurs through oxidation. Oxidation is a natural process that can be accelerated by mechanical stress, temperature, entrained air, electrostatic discharge and metal particles [22].

These degradation influences are found in most mechanical environments. As oil begins to degrade varnish precursors are formed such as acids, alcohols, and water. These precursors react with oil in the system and, at the right environmental conditions, will precipitate out of solution. Varnish molecules are polar and adhere to metal surfaces creating a film. Varnish usually has a gold – orange appearance that darkens as the film thickens, although appearance changes with chemistry and operating environment [9].

1.4.2.1 Lubrication oxidation

Oxidation is a part of the natural aging process of a lubricant. This oxidation process reveals itself as discoloration and odor change. As the oxidation level increases, the viscosity of the oil will also increase until a critical level is reached, and the oil must be replaced. Oxidation degradation of lubricants leads to the formation of various oxygen containing compounds that, in higher concentrations, can polymerize into sludge or varnish. Varnish precursor molecules consist of esters, ketones, peroxides, alcohols and acids [9]. The oxidation of hydrocarbon lubricants is assumed to occur by the free radical chain mechanism. The free radical chain mechanism is made up of a two-step process. The first step involves the hydrocarbon molecule to being cleaved thermally and forming an organic radical. This step can accelerate oil degradation as free radicals react and propagate to the lubricant. In the second step oligomers are formed leading to the formulation of sludge and varnish as molecular weight increases.

1.4.2.2 Heat

The primary cause of oil degradation is heat. In every system there are points at which the thermal stability of the oil (lubricant) is exceeded. It has been observed that for every 10° C increase above 100°C in operating temperature the oxidation rate doubles (Arrhenius rule)[26]. As modern vehicles become more efficient by increasing the operating temperature, it is becoming harder to find lubricants that maintain a low oxidation rate at these higher temperatures. There are other causes of heat in a mechanical system, such as micro dieseling, which describes entrained air bubbles that collapse when passing through high-pressure regions of a system. This phenomenon can create local oil temperatures that exceed 1000° C. Static charge also contributes to hotspots in a lubrication system. As oil flows through a synthetic filter, charge buildup can be released in a spark. These intense static discharges can have local temperatures of up to 10,000°C, fragmenting oil molecules and creating free radicals [27].

1.4.2.3 Metal catalysis chain initiation

Lubricants in a large system have many tasks. One of them is to carry particulate matter away from moving surfaces. These wear particles are usually metal containing iron and play a critical role in the chain initiation process of lubricant oxidation. This auto catalysis process can take one of two forms and is usually initialized by oxygen, high energy light or mechanical stress [28].

$$RH + O_2 \rightarrow R\cdot + HOO\cdot \qquad (1\text{-}7)$$

$$2RH + O_2 \rightarrow 2R\cdot + H_2O_2 \qquad (1\text{-}8)$$

These interactions proceed very slowly until temperatures reach 100°C or higher. The bonding of the hydrocarbon molecule dictates how easily it can undergo degradation through these reactions. Some molecules present in oils, such as aromatics, are most easily oxidized. Hydroperoxide decomposition reactions are a second kind of initiation reaction that can occur at a much lower temperature. These reactions utilize impurities in the system as a catalyst, usually metal ions and wear particles that have been suspended in the lubricant.

$$Fe^{3+} + ROOH \rightarrow Fe^{2+} + ROO\cdot + H^+ \qquad (1\text{-}9)$$

$$Fe^{3+} + ROOH \rightarrow Fe^{3+} + RO\cdot + H^{-} \quad (1\text{-}10)$$

The hydroperoxide levels will increase as the lubricant ages until a critical point when the hydroperoxide decomposition initiation reaction dominates the degradation of the lubricant [17].

1.4.2.4 Chain propagation

Chain propagation involves the reaction of the substrate with oxygen gas to produce additional radicals that can propagate the oxidation reaction in the lubricant. The peroxyl radical robs the hydrogen in other hydrocarbon molecules and produces hydroperoxides and alkali radicals.

$$R\cdot + O_2 \rightarrow ROOH + R\cdot \quad (1\text{-}11)$$

$$ROO\cdot + RH \rightarrow ROOH + R\cdot \quad (1\text{-}12)$$

Due to a low activation energy, the initial chain propagation reaction occurs quickly. The next step occurs much slower as hydrogen is robbed from existing hydrocarbon chains. The hydroperoxide breaks down into two radicals.

$$ROOH \rightarrow RO\cdot + HO\cdot \quad (1\text{-}13)$$

These free radicals react with the lubricant molecules create new free radicals, alcohols and water.

$$RO\cdot + RH \rightarrow ROH + R\cdot \quad (1\text{-}14)$$

$$HO\cdot + RH \rightarrow H_2O + R\cdot \quad (1\text{-}15)$$

The lubricant auto catalysis oxidation process follows this pattern and ultimately leads to sludge and varnish deposits in the system. First the formation of aldehydes and ketones occurs. These are unique chemical species in the oxidation process that lead to the formation of oligomers, polymers, and eventually sludge and deposits. Condensation reactions increase the molecular weight of forming varnishes. As the antioxidants in the lubricant are overwhelmed, this process accelerates and large deposits are formed [28].

1.5 Varnish removal

A typical turbine lubrication system will have a mixture of varnish deposits and varnish precursors in the oil. This occurs because oil has a limited solvency for varnish. Varnish and sludge formation adversely affect the efficiency of engine operation by increasing viscosity, reducing tolerances between precision parts, and by reducing flow at bottleneck regions in lubricant system. The lubricant system will need to be cleaned by removing suspended varnish and varnish precursors from the oil. This will in turn allow deposits to be dissolved from the metal surfaces. There are numerous methods for removing varnish from lubrication systems, including: chemical cleaners, electrostatic charge induced filtering, adsorbent medium and additive stabilization [29]. Many systems employ a last chance filter aimed at removing varnish

precursors upstream of the valve systems. Last chance filters are extremely fine pored (2-4µm) and are susceptible to clogging [17].

1.5.1 Additives and synthetic oils

One avenue to remove varnish from a system is to prevent its formation. Techniques in the refining of oil have been found to combat thermal and chemical degradation of the lubricants in operation. Synthetic oils are produced with fully saturated chains that are resistant to oxidation at higher operating temperatures. The fully saturated chains have no bonding sites and therefore are less interactive with foreign particles produced during use. Additives are antioxidants that create a buffer that allows oil to be used for longer without oxidation[30]. These antioxidants and buffers maintain the acidity level of the oil and reduce acceleration of oxidation. One drawback to additives is that they can have a high environmental impact, making disposal difficult.

1.5.2 Electrostatic removal

Electrostatic absorption takes advantage of the polarity of varnish to remove varnish and varnish precursors from the oil while in operation. This usually occurs outside of the main lubrication loop or in a kidney loop off the main reservoir. To remove the particles, oil passes through a high electrostatic field where the polar molecules are attracted to the opposite charge and removed from the oil during circulation, as illustrated in Figure 1-6[14]. As the electrostatic filter reduces the concentration of varnish and varnish precursors from the lubricant, previously precipitated deposits can be reabsorbed into lubricant. Over time this can reduce overall varnish deposits in the system. Electrostatic filters are susceptible to increased levels of moisture and wear particles that can interfere with absorption plates in the filter system [17].

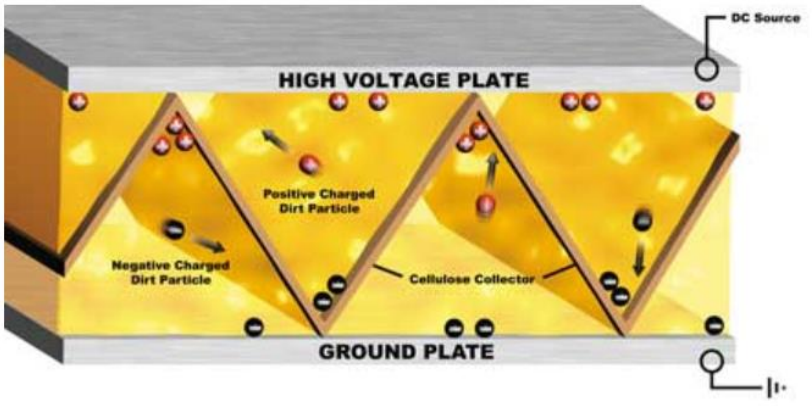

Figure 1-6: Schematic of an electrostatic filtration system. The large electrical field attracts suspended varnish molecules and varnish precursors out of the lubricant as it passes through the system [31].

1.5.3 Absorption filter

A filter can be placed into the lubricant circulation loop to remove varnish particles, as shown in Figure 1-7. The absorption media has high surface area and a high void volume to increase interaction with the lubricant. Many different materials are used as filter media, but the majority have a microporous structure or linear crosshatching assembly[14]. Many of the materials used in the filters have an affinity for polar varnish precursors. Absorption can happen in two different forms, chemical absorption and physisorption[31]. In chemical absorption, a chemical bond is formed between the varnish precursor and the filter media. In physisorption, precursors are held by weak van der Waals forces and hydrogen bonding. The primary drawback to filter media is potential for clogging, and the small pore size may damage the lubricant by removing additives

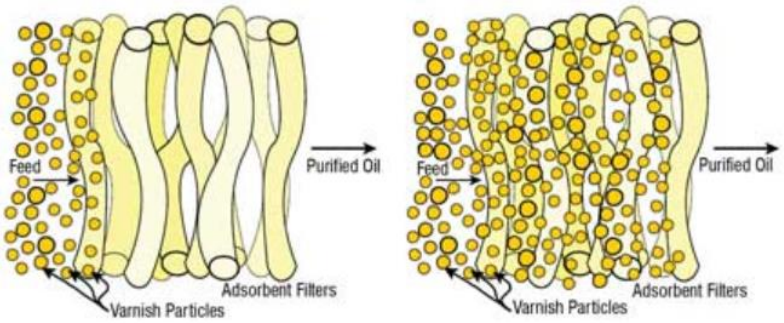

Figure 1-7: Varnish filtration through absorption media [31].

1.5.4 Chemical cleaners and flushes

The flushing method removes varnish by replacing primary lubricant with a chemical cleaner that softens and removes deposits in the system. The chemical cleaners remove deposits that are insoluble in solution. They then suspend the small particles in the cleaning fluid, where they can be filtered out of the fluid. The process of chemical flushing can take hours or days depending on efficiency and volume of deposits. The chemical cleaners must be flush from the system before operation is resumed to ensure no damage occurs to the new lubricant in the system. Chemical cleaners are used as a last resort and require a system to be taken off-line for service, which adds costs and lowers productivity. The benefit of chemical cleaners comes in their quick removal rate[14]. Even though a system must be shutdown, service is relegated to a short period of time and can be cost effective. This thesis will focus on the chemical cleaner approach to varnish removal.

1.6 Summary

In a previous study of varnish removal using chemical cleaners [14], a test rig was constructed that enabled real time measurements of varnish removal. The development of this test rig was one of the primary goals of the earlier study, providing a controlled environment where temperature and flow could be adjusted, and visual data captured. The characterization of aging

varnish was used to measure the relationship between oxidation level and removal characteristics. That work was not only valuable to ensuring consistency of results obtained with the test rig but for industrial estimates of varnish removal times. Commercial comparisons of chemical cleaners' effectiveness at removing high oxidation level varnish in a high flow regime were run as a proof of concept and for commercial value. However, there was no systematic comparison of different chemical cleaners and their concentration in the base oil, or of operating conditions, including flow rate and temperature. Also, the properties of the varnish removed from the oil and trapped in the filter were not characterized.

The goals of this study were to expand the commercial studies to a low flow, low oxidation regime which is relevant for large flow channels and sump regens of a lubrication system, and to investigate the effects of cleaner concentration, temperature, and flow rate on varnish removal. These tests not only allow us to investigate the physical phenomenon of varnish removal but also increase the precision of the characterization device. In Chapter 2, the test rig and test procedure are described in detail, with emphasis on the new contributions made through this study. Chapter 3 describes the test results, including varnish removal times and filter analysis for different cleaners, cleaner concentrations, temperatures and flow rates. Numerical simulations of fluid flow over the varnish are also reported. Lastly, Chapter 4 summarizes the contributions of this project and suggests future research directions.

2 Experimental Design and Methods

2.1 Test rig

The test rig was designed to provide a controlled environment to test chemical cleaners' efficacy in varnish removal. To provide this environment, the flow needs to be continuous without variation throughout testing and the working temperature of the test apparatus should be able to be consistent throughout the circulation of fluid, with only slight variations from the target temperature. The test apparatus was built to accept coupons containing artificial varnish that was formulated to match gas turbine engine varnish. These varnish coupons were tested in the no slip region of the flow, mimicking the actual engine environment. The fluid reservoir for the test apparatus was built to minimize excess fluid but maintain a ratio of varnish to chemical cleaner, reproducing a typical working environment.

The test rig used throughout this study is shown in Figure 2-1. This test rig was already built at the start of this project but was modified during the project to improve the accuracy of testing and ease of use of the test rig. Specifically, the test rig was improved to allow air to be cleared from the filter, ensure the varnish was not exposed to flow higher than the test parameters and all assembly is downstream and side stream to the test cell, and that laminar flow could be maintained throughout the test.

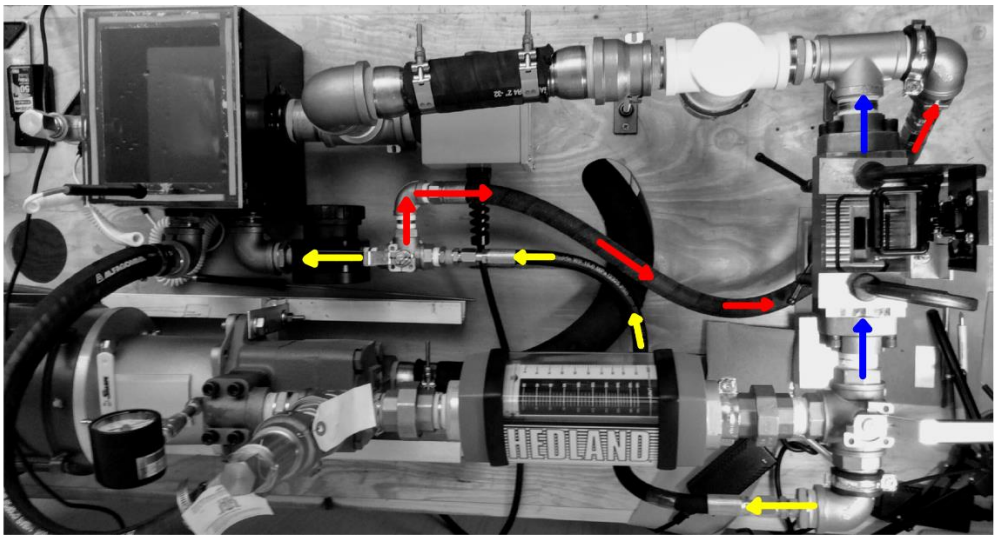

Figure 2-1: Top view of the test rig. Blue arrows indicate the direction of flow during test. Yellow arrows indicate diversion A through the positive displacement flow meter. Red arrows indicate diversion B, where high flow is diverted around the test cell to flush air from the filter

2.1.1 Existing test rig features

Consistent flow over the varnish is paramount for reproducible experiments. A positive displacement pump, which moves a volume of fluid from an inlet to an outlet creating flow, is the best option for this application. To simulate the operating conditions in an engine, the test apparatus produces Reynolds numbers ranging from 0 to 6000. This allows for study of varnish removal in laminar and turbulent regimes. The pump needs to be able to supply chemical cleaner efficiently at a volumetric flow rate of 0 – 46 GPM. A rotary vain pump was selected for these parameters. Specifically, the test rig has a positive displacement pump that uses centripetal force to seal piston against the exterior of an oval cavity. The circular motion transfers fluid from the inlet to the outlet creating a measured flow.

The test cell port geometry is designed to expose varnish to well-developed pipe flow at the no slip boundary, while minimizing turbulence. To accomplish this, the port geometry is a rectangular semi-circle shape, the width of the varnish. This exposes the entire surface of the varnish equally to fluid flow without exposing the varnish edges to flow.

The test apparatus is required to have a temperature range from 20° C to 120° C. The heating element with this capacity is installed in the return line just before the reservoir. The test apparatus is not insulated and uses iron pipe. Even with heat diffusion and convection, the chemical cleaner has a relatively short distance to circulate, so the fluid temperature is consistent throughout the circulation, even at low volumetric flow rates.

The system is designed to accept varying chemistries of chemical cleaners without damage. The complete volume of the system including pump, test loop, pressure relief loop, and diversion loop is just over 5 gallons. The test reservoir is 3 gallons. The small reservoir is the minimal size to allow for air to escape while circulating chemical cleaners. As the chemical cleaner removes

varnish it is incorporated into the fluid and circulated through the test apparatus. A filter located downstream of the test cell removes varnish particles from the fluid for later study. The filter is a 15 µm steel mesh filter with an inner layer of nylon 5 µm filter cloth.

Varnish is specific to the engine application and the oil formulation used in the system. The test cell is designed to accept a flat uniform coupon of set dimensions. The varnish is deposited on an inner rectangle of the coupon that fits into the flow channel. The coupon system allows for testing of various varnish formulations. The varnishes are developed using ASTM standards. Varnish samples are stored in base oil or inert gas to minimize continued oxidation and varnish hardening. All test samples are generated from the same batch of varnish to ensure consistent chemistry and oxidative response.

The test cell is designed to house the varnish coupons during a test and to enable imaging of the varnish as it is removed. As shown in Figure 2-2, the cell has a lid that was manufactured from poly carbonate that is vapor polished to allow visual data to be retrieved during tests. The test lid dimensions were redesigned in this project to eliminate thermal expansion locking at high testing temperature.

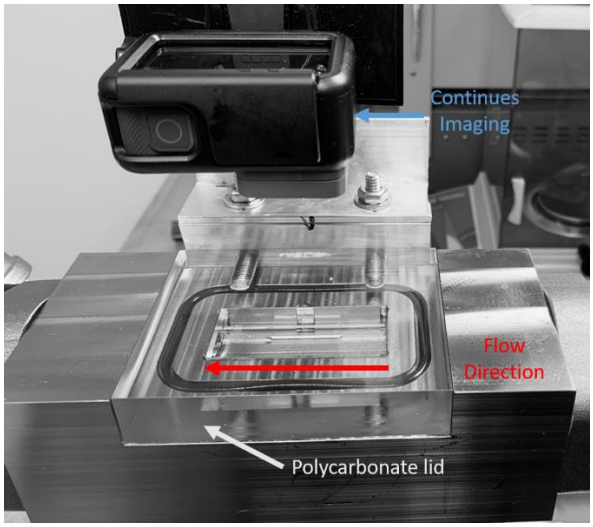

Figure 2-2: The test cell assembly including the polycarbonate lid and imaging camera. The flow direction is labeled with a red arrow.

2.1.2 Test rig enhancements

The test rig is operated without the benefit of the fume hood. During the circulation and heating process, the fluid is in a sealed environment where aromatics and volatile molecules cannot be released into the air. However, molecules can be released at the reservoir, where the system is not completely sealed from the open air. Therefore, when operating the test system at or above 90° C, or during the cleaning out process, the ability to filter air entering the room from the test reservoir was necessary. To achieve this, a rigid lid with the seal was designed to allow fumes to escape from a single region of the reservoir. A portable fume extractor with a two-stage filter was identified and purchased, shown in Figure 2-3. The first filter is a HEPA filter with the

capability of removing particles of 0.3 µm and larger. The second filter is an active carbon filter and is efficient at removing acids and chemical species from the air.

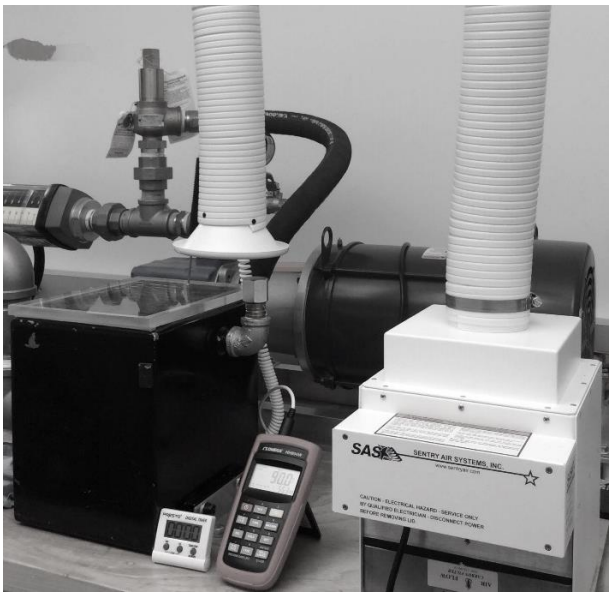

Figure 2-3: Thick poly (methyl methacrylate) reservoir lid with seal and sanitary air system

The test requirements for the rig were extended to include long-duration tests, up to 140 hours. Due to the position and set up of the test rig, these long tests could not be run continuously. So, a new procedure and rig configuration were needed to allow the startup and shutdown of a continuous test without artificially influencing varnish removal. Four primary constraints were considered. First, the flow profile through the test cell must not be altered. Second, once a test begins, the varnish cannot be exposed to a higher volumetric flow then the test parameter. This precaution would ensure that varnish was not artificially removed from the coupon during the startup and cooldown procedure. Third, the entire test rig must be at thermal equilibrium before start of test. This ensures that the fluctuation of temperature from the thermostat does not move out of the specified parameters. The viscosity of the oil is highly dependent on the temperature. If the rig is not at thermal equilibrium there can be high fluctuations in volumetric flow rate and temperature, severely affecting results. Finally, all air must be evacuated from the downstream filter. If air is present in the filter housing it will affect the ability of the cloth filter to seat, allowing particle bypass. This can influence the particle count results.

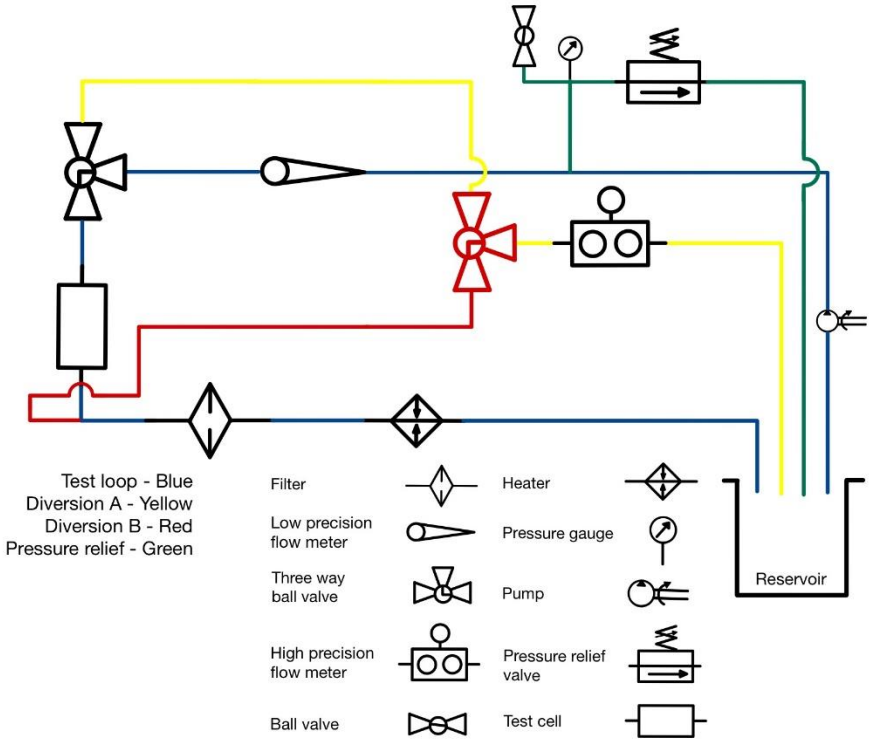

Figure 2-4: Schematic of the test system including additional upgrades marked in red. The primary test loop is marked in blue, diversion A, (in yellow) diverts flow through the high precision flow meter, diversion B completes the loop bypassing the test cell.

To enable long duration tests and meet the constraints identified above, the original test rig was modified. Diversion B, shown in Figures 2-1 and Figure 2-4, diverts flow parallel to the test cell and rejoins the test loop downstream of the test cell. This configuration minimizes the effect on the flow profile. When all flow is diverted down diversion A and back up diversion B, hydrostatic pressure ensures that flow is not induced in the clockwise direction through the test cell. This also allows high flow rates to be diverted through the downstream portion of the test loop, clearing air from the filter and seating the filter cloth against the mesh filter housing. Diversions A and B give the operator the capability to heat all portions of the test rig to test temperature, except the test cell, prior to testing.

2.2 Test procedure

2.2.1 Varnish storage and preparation for testing

Varnish samples are sealed in polymer containers with inert gas to reduce oxidation during storage as shown in Figure 2-5. Before each test, the varnish coupon is removed from its sealed container and weighed. The mass measured in the lab is used for posttest analysis. Each

component of the test, fluid, filter and coupon is imaged for posttest analysis. The images are taken in consistent lighting with a white background.

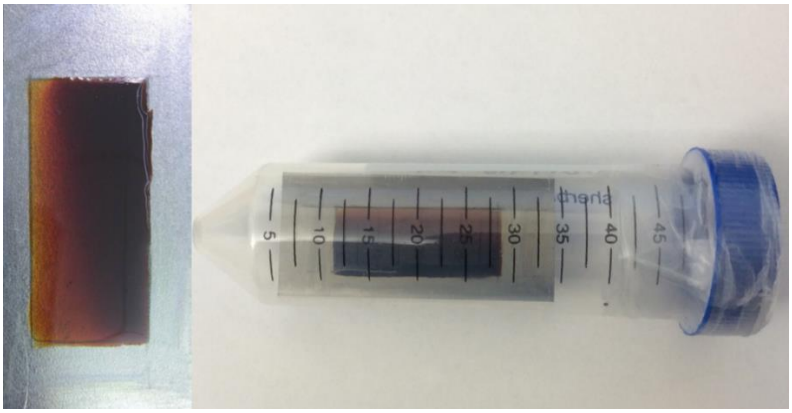

Figure 2-5: Coupon storage in inert gas in preparation for pretest.

The test apparatus must be flushed of all cleaning fluid from previous tests before use. An un-formulated base oil is circulated for five minutes to remove any residual cleaner. During this flush step, the pressure must be increased to over 120 psi to evacuate the pressure relief valve and diversion line. The base oil is then drained from the system and compressed air is used to remove the maximum amount of oil from the system.

2.2.2 First day/single day startup

The apparatus is filled with the new test fluid and the test temperature is set. The test fluid must be circulated while it is heated. This ensures that local area of fluid is not above its denaturing temperature and speeds up the heating process. During the initial warm-up of a rig, all components should be heated to a homogeneous temperature before the test. This will ensure that flow and thermostat temperature remain within test parameters. Once the rig has reached the test temperature, the flow is stopped. The test cell is opened, and the polycarbonate lid is inserted with the test coupon. The cameras are inserted, and lighting is optimized.

When the rig is restarted, all flow is diverted through the positive displacement flow meter diversion (diversion A). This is continued until all foam has dissipated from the fluid. After the foam is dissipated, a small amount of fluid < 0.5 GPM is flowed through the test cell to evacuate the air. This process usually takes a up to two minutes to evacuate air from the test cell, filter and return loop. Once the test cell and most of the pipe are full of cleaning fluid, all the flow is first diverted back into (diversion A) and then diverted to (diversion B). This step clears the filter of any residual air left in the filter while hydrostatic pressure protects the varnish from the high flow rate. The test is now ready to start. Flow is diverted through diversion one and calibrated to a specified flow rate. The desired flow is then directed through the test cell. Time lapse photography is started with the 12-megapixel image every 10 seconds. The temperature is averaged throughout the test and should not exceed a variance of 5°C from the test specification.

2.2.3 Multi-day startup

When a test is run for multiple days in succession, the startup and shutdown of the rig is important for continuity. Two procedures were used for multi-day tests. In the first, the coupon is removed from the test cell in a standard shutdown procedure and stored in base fluid overnight. The coupon is then reinserted into the test cell in the morning after a normal startup procedure.

In the second procedure the coupon remains in the test cell for the entire duration of the test. The warm up procedure starts by setting the test temperature and circulating fluid through diversion A. Once the temperature is within 20% of test parameter the flow is changed to diversion B. This allows the remaining fluid volume in the return loop to be brought up to temperature and heat the external piping. The flow can be alternated between diversion A and diversion B to ensure most of the rig is at test temperature before the test is started. The only part of the rig that is still below test temperature is the test cell. To ensure the effects of shear force and flow rate are consistent, a small amount of fluid ~0.1 GPM is flowed through the test cell until it is at or close to test temperature.

To start the test, first all flow is diverted through diversion A. The flow is adjusted so that when diversion to the test cell happens, an easily recognizable number is still flowed through the positive displacement flow meter. At this time the desired flow is diverted through the test cell, time-lapse imagery is activated, and the test is resumed.

2.2.4 End of test process

At the end of a test, time lapse photography is stopped. All flow is diverted to diversion A. The pump is turned off and thermostat is set to zero. The polycarbonate lid is removed from the test cell and the coupon is carefully removed.

Images are taken of the coupon directly after removal from the test cell at zero and 10 times magnification. The 5 µm filter paper is removed from the downstream filter housing and imaged at zero, 10 and 20 times magnification. An example is shown in Figure 2-6.

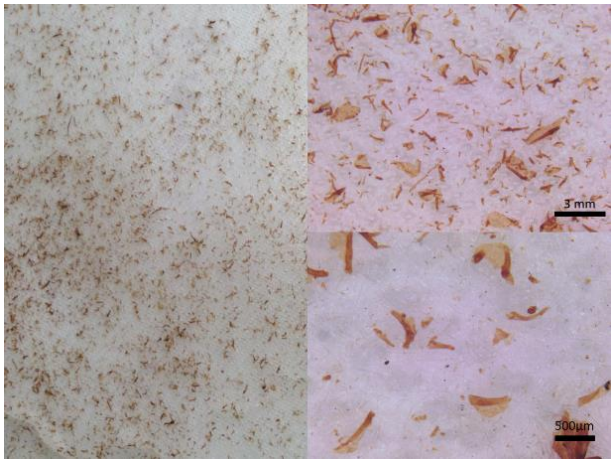

Figure 2-6: Filter images at zero (left), 10 (upper right), and 20 (lower right) times magnification.

The coupon is rotated slowly in heptane for 10 seconds to remove oil. The coupon is then dried using compressed air. The compressed air should be at a low air pressure to reduce damage to the varnish. The coupon is weighed for comparison to the start of test weight. If the removal fluid has diffused into the varnish, the coupon may need multiple heptane washes to remove the maximum fluid from the coupon. The coupon should not be rotated in the heptane after the first rinse. The varnish becomes very brittle after exposure to heptane and will be artificially removed from the coupon which will change the end of test weight. Instead the coupon is slowly removed from the heptane allowing cleaner fluid removal without removing varnish. A representative image of a coupon before and after the heptane wash is shown in Figure 2-7. The coupon is weighed and recorded for posttest analysis. Each coupon is weighed again at least 24 hours after test to confirm that additional weight is not lost due to evaporation of cleaner fluid. Finally, time-lapse photography is downloaded and prepared for postprocessing.

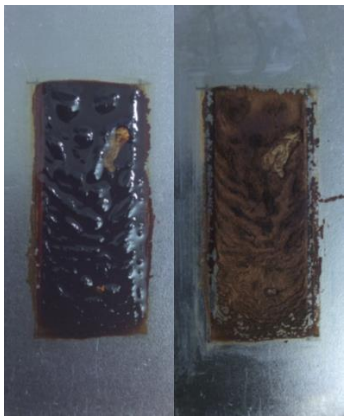

Figure 2-7: Varnish coupon before and after heptane rinse.

2.3 Visual varnish removal analysis

Visual data in the form of time lapse photography is processed to give real time measurements of varnish removal. All images are taken from above and imaged the coupon through the polycarbonate lid and cleaner fluid. This requires a normalization to allow for comparable data. To process the images, the CMKY color scale is used. The primary color used is K because it represents the darkness of the image and can be correlated to varnish removal. The varnish is a semi-opaque dark brown polymer that reveals the steel coupon gradually as it is removed. To correlate the K value of removal, we average the K values over specific regions of each image. Each pixel in these regions has a K intensity value between 1 and 255. The average K value of the region is calculated then divided by 255 to give an average percentage K value.

To identify the minimum and maximum K value for a given coupon and fluid, the primary image is cropped in two ways. The minimum value is taken from a cropped image of the steel and the maximum from a cropped image of the pre-test varnish, as shown in Figure 2-8. The K values in these cropped regions are determined from the first 100 images processed. The varnish crop should encompass as much of the varnish surface as possible to be a fair representation of varnish removal. This is essential if the varnish is heterogeneous in its thickness or surface texture. The other accommodation that must be considered when making a varnish crop is the maximum average K value, which should be as dark as possible. If there are regions of thin varnish that can be excluded without reducing the overall area substantially, that should be accommodated for. The steel crops determine the lower bound of the removal graph. The steel coupon represents the point where no varnish is left. To best represent the minimum average K value for the test, two crops are made. One on either end of the varnish representing the inlet and outlet of the fluid. The two steel crops should cover as much surface area as possible without incorporating lighting artifacts or distortions. The minimum K value is taken as the average for the two steel crops to account for small differences in lighting from one end of the coupon to the other, which results in a consistent lower bound.

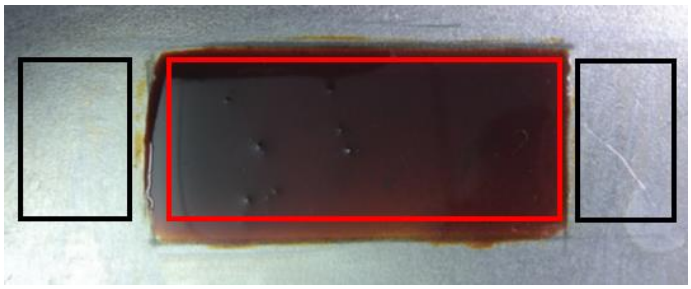

Figure 2-8: Two regions on the coupon (in red and black rectangles) that are cropped from the images for post-processing and calculation of varnish removal.

To normalize each test and enable comparison from test to test, the upper and lower bound are used. This eliminates the influence of fluid color and lighting differences.

$$K_{normalized} = \frac{K_{varnish\ average} - K_{steel\ crop}}{K_{varnish\ maximum} - K_{steel\ crop}} \qquad 10$$

The normalized K values can be plotted against time producing a varnish removal graph. A representative result is shown in Figure 2-9. The primary points of interest are 10% removal and 90% removal. This indicates the point at which the fluid begins to remove varnish and approximately the time of total removal. These values will be used to compare different varnish removal conditions.

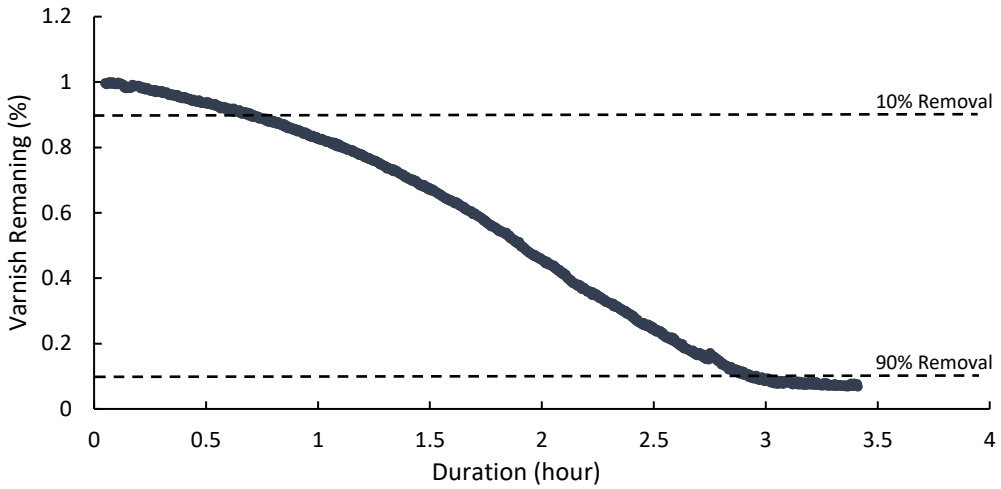

Figure 2-9: Representative plot of varnish removal as a function of time obtained by post-processing images of the coupon taken during the test. The 10% and 90% removal times are identified by dashed lines.

2.4 Particle analyses

Particle data is analyzed from the 5 µm filter cloth that is positioned downstream of the test cell. The 10 times magnified images are used for this analysis. The filter cloth is white and the varnish that is removed from the coupon is a dark amber color, providing a large contrast for image processing. An algorithm was developed to count and measure the particles. For this analysis RGB color scale was used due to its versatility in binary image conversion threshold [32]. To ensure that a representative sample was taken from each filter, three images were used from different locations on the filter.

For image processing each filter image is converted into a binary map. The image is first sequenced for the three colors, red, green and blue. Matlab can provide an automatic gray threshold but this value may lead to artifacts in the binary image. Inspection of the original image is necessary to ensure the binary image is as accurate as possible. Once a binary image is as accurate as threshold manipulation can achieve, the holes in the particles are filled in to completely define the regions of zeros and ones. Most of the images will still have light diffraction around the edge of each particle. This effect is exacerbated by the residual oil left on

the filter. To eliminate diffraction artifacts around the large particles, any particles having a diameter less than 50 µm are eliminated. An example image shown at different stages in this process is shown in Figure 2-10.

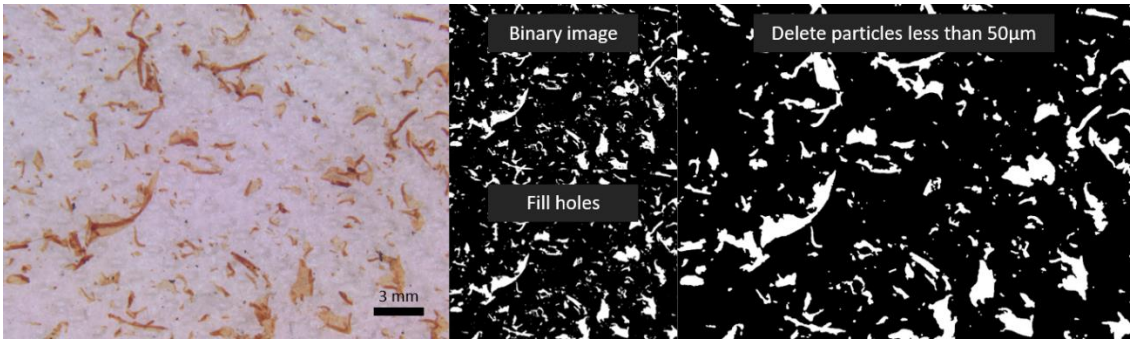

Figure 2-10: The succession of steps (from left to right) to convert a 10x magnified filter image into a measurable binary image.

Several particle properties can be compared: particle fill area, equivalent diameter, and maximum axis length. Particle fill area returns the number of pixels in each particle region. Equivalent diameter creates a circle of equal area to the particle and returns the number of pixels across the diameter. Major axis length creates an ellipse with the same central normalized moment as the particle and returns a pixel length for the major axis [33]. The major axis metric is shown on a representative sample in Figure 2-11.

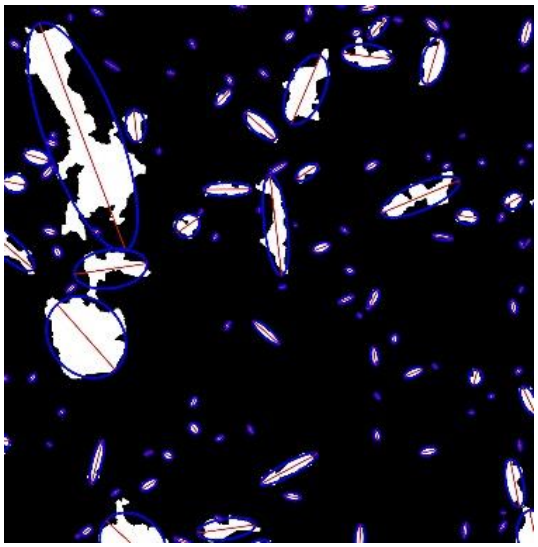

Figure 2-11: Particle area is calculated by counting the number of pixels or and shape are quantified as the major axis of an ellipse that defines each particle.

These three measurements are converted into millimeters squared or millimeters and a histogram is created. The histograms for equivalent diameter and fill area should be similar, with two orders of magnitude difference. The major axis length histogram may have a different shape depending on the geometry of the particles on the filter. The three-primary metrics for particle data is the number of particles, maximum particle length, and the root mean squared of

the major axis length histogram. These values are recorded for each test and evaluated to identify trends or correlations.

3 Results

3.1 Test Summary

Chemical cleaners are used to remove varnish at a range of different operating conditions, including different temperatures, flow rates and at varying concentrations. Therefore, it is necessary to characterize the effect of these conditions on varnish removal. A complete list of tests performed during this study is provided in the Appendix. First, six different commercial cleaners were tested and compared at a set operating temperature and flow rate. Then, for one of these cleaners, the temperature, flow rate and concentration were varied to understand the effect of these important parameters. The temperature was varied from 60°C to 100°C with an interval of 10°C; flow rates were tested at 0.1, 0.5, 1.0, 1.5, 2.0, and 4.0 GPM; and the chemical cleaner was mixed with base oil at concentrations of 5%, 10%, 15% and 20%. The chemical cleaners used in these tests were proprietary, so detailed chemical composition analysis is not available. However, it is known the chemicals were blended with a 46 cSt (at 40°C) base oil. Also, the viscosity of the final formulation was measured to be 46.62 cSt at 40° C and the viscosity index was 104. Using the flow rate, temperature and viscosity, the Reynolds number was calculated for all tests and found to range from 73.9 to 2956, indicating that the flow was in the laminar regime for all tests except 4.0 GPM.

For each test, the varnish removal process was characterized in terms of multiple metrics. First, the appearance of the coupon after the test was analyzed in terms of the texture of the surface, visual assessment of the removal amount, and the uniformity of the surface after removal. Second, the amount of varnish removed was characterized from the difference between the start and end of test weights of the coupon. Next, filter images were used for visual analysis of the appearance of particles, presence of rolled up sheets or small rigid particles, and appearance of trends in particle size. Analysis of the particle distribution across the entire filter was used to assess the viability of the filter data. A generally homogeneous distribution was indicative of a good filter seal where most particles 5 µm or larger were captured and evenly spaced on the filter. If the filter was not sealed properly, particles clumped in small regions of the filter rendering filter analysis unusable. Digitalization of the particle images was then used to characterize the root mean squared of the particle size and trends across particle counts. Lastly, and possibly the most important metric, the rate of change of varnish removal as a function of time was analyzed and the time required to remove 10 and 90% of the varnish reported.

The duration of each test was dependent on how long it took to reach at least 90% varnish removal. Durations varied from 2.5 hours to 142 hours. These long durations meant that multiple tests could not be performed at each test condition. However, one condition was tested multiple times: 0.5 GPM, 90°C and 20% cleaner concentration. It was found that the

variation in 10% removal time was +/- 2.3 minutes and 90% removal time was +/- 8.2 minutes. The particle size data also exhibited some variation across the tests, with the root mean square size of the particles having a variation of +/- 0.38mm This variation is primarily attributable to slight differences in the initial amount and distribution of varnish on the coupons. For example, the weight of the varnish on the coupons used in this testing was targeted to be 80 mg but varied between 66.5mg and 97.3mg. Although variation of test results was only analyzed for one condition, we assume that the error calculated for this condition is approximately the same as for other test conditions. In future research, this assumption could be tested, in case the variation is dependent on test conditions.

3.2 Commercial Cleaner Tests

We compared six different commercially available chemical cleaners, referred to as fluids A through F, for their effectiveness in removing varnish. These tests were performed at a constant temperature and flow rate of 90° C and 0.5 GPM, respectively. Each test was run until either 90% removal was reached or 40 hours of test time had elapsed. Upon completion of each test, the coupons were inspected for removal characteristics. If significant varnish removal occurred, particle analysis was performed on the downstream filter and a removal curve was generated from visual time-lapse data.

In Figure 3-1, we see that fluid A and fluid E have significant varnish removal during the test. Fluid A has characteristic patchy regions that indicate large particle removal, whereas fluid E cleaned regions of the coupon down to the steel with very little evidence of residual particles. Fluid B and fluid D have no visual change after 40 hours of testing. Fluid C and fluid F appear to have softened the varnish to a point that the shear stress extended the varnish in the direction of flow, yet there appears to be very little varnish removed. Table 3-1 corroborates a visual inspection of the coupons for fluid A, though F with only slight variations.

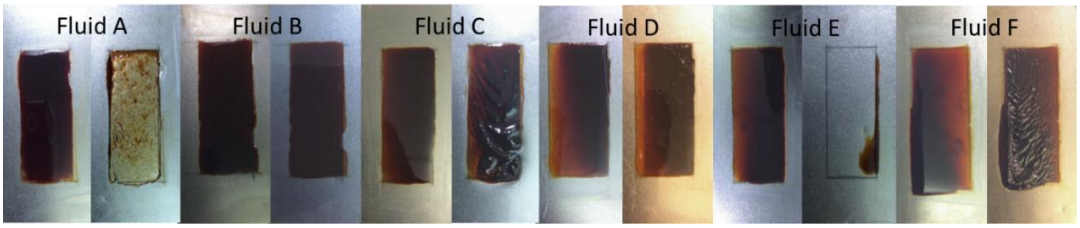

Figure 3-1: Test coupons at the beginning and end of testing. The flow direction for all tests coupons is from top to bottom on the page. The test parameters were held constant for all tests at 90°C and 0.5GPM, for temperature and flow rate, respectively.

Table 3-1: The coupon weight before and after test for each temperature tested.

Fluid	Pre-test weight (mg)	Post-test weight (mg)
A	80.2	5.7
B	77.5	59.0
C	76.4	74.9
D	84.6	76.4
E	80.1	2.4
F	89.4	79.8

Visual inspection of the filters in Figure 3-2 shows that there was only significant particle accumulation for fluid A. The varnish removed by fluids B through F was smaller than the pore size of the 5 µm filter. Fluid E shows very different removal characteristics than fluid A, dissolving the varnish into the cleaner fluid. Fluid A has an average particle size of 410 µm and could be filtered out the cleaning system without requiring hot flush, yet downstream clogging of low tolerance parts could occur. Fluid E has an average particle size below 5 µm and would be difficult to filter from the system resulting in a hot flush of the cleaner fluid from the lubricant system to remove the varnish.

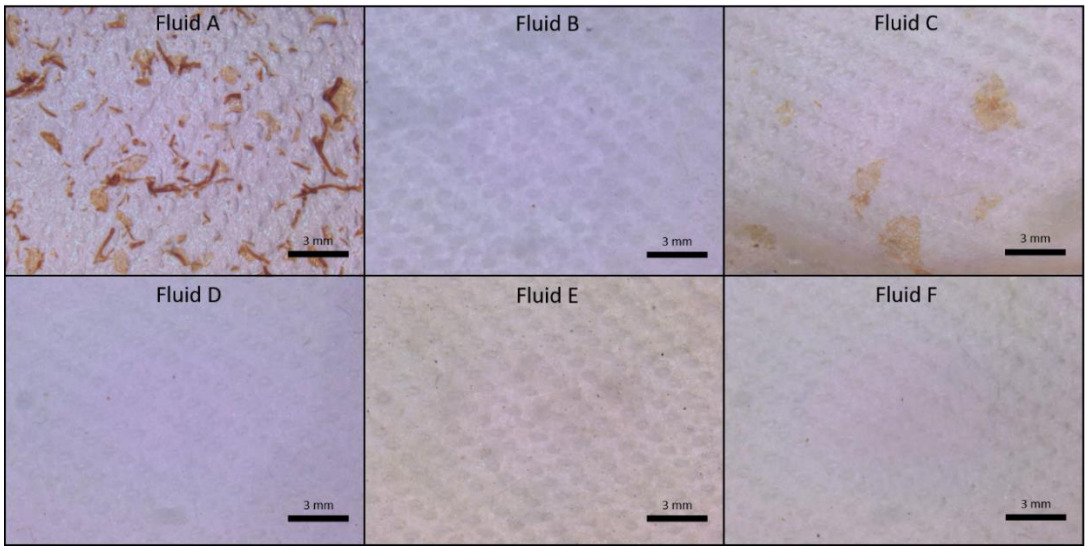

Figure 3-2: Optical microscope images of the posttest 5 µm filters with accumulated varnish particles at 10x magnification.

Figure 3-3 shows the visual removal curves for fluids A through F. As we can see from the graph, only fluid A and fluid E had significant removal. The remaining fluids remained at steady-state for the entire 50-hour test. Fluid A removed 90% of the varnish in 3.21 hours +/-8 minutes and fluid E removed 90% of the varnish 3.93 hours +/-8 minutes.

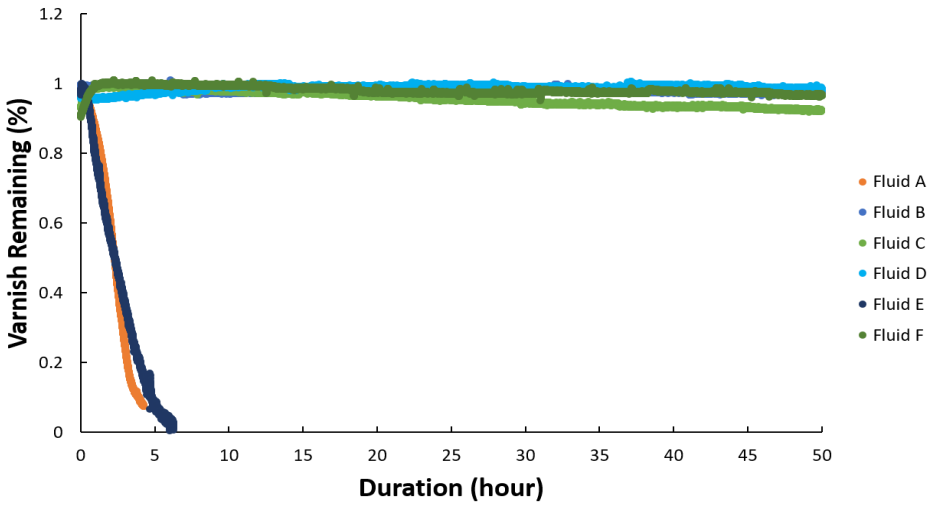

Figure 3-3: Varnish removal for fluids A through F. For each of these tests the temperature and flow rate were held constant at 90°C and 0.5 GPM, respectively.

There is a discrepancy between the visual removal data in Figure 3-3 and the varnish mass data shown in Table 3-1 for some fluids. In particular, in terms of varnish mass, fluid C removed 24.4% of the varnish, while it removed 2.7% according to the coupon images. This is analyzed further in Figure 3-4 which shows the removal percentage for mass loss in the visual data mass loss. The inset graph shows the K value calculated from the time lapse photography in the first 30 minutes of the test. The K value increases from 0.91 to 0.97 in the first 30 minutes which implies a mass increase on the coupon.

The first step of mechanochemical removal of the polymer is to change the configuration of the polymer chains which can have a mechanical, configuration or visual effect[23]. This causes darkening of the varnish during the initial stages, masking early removal. This darkening effect is negligible for tests with substantial removal due to the thinning of the varnish that allowed the steel coupon to shine through and give a reasonable end of test results. However, when the total removal is small, the precision of the visual processing data is decreased. This is a limitation of the accuracy of the test approach for cleaners that remove very little varnish.

All subsequent analyses reported in this chapter were performed with fluid A, which removed significant varnish. Therefore, the accuracy limitation mentioned above should not be a significant issue.

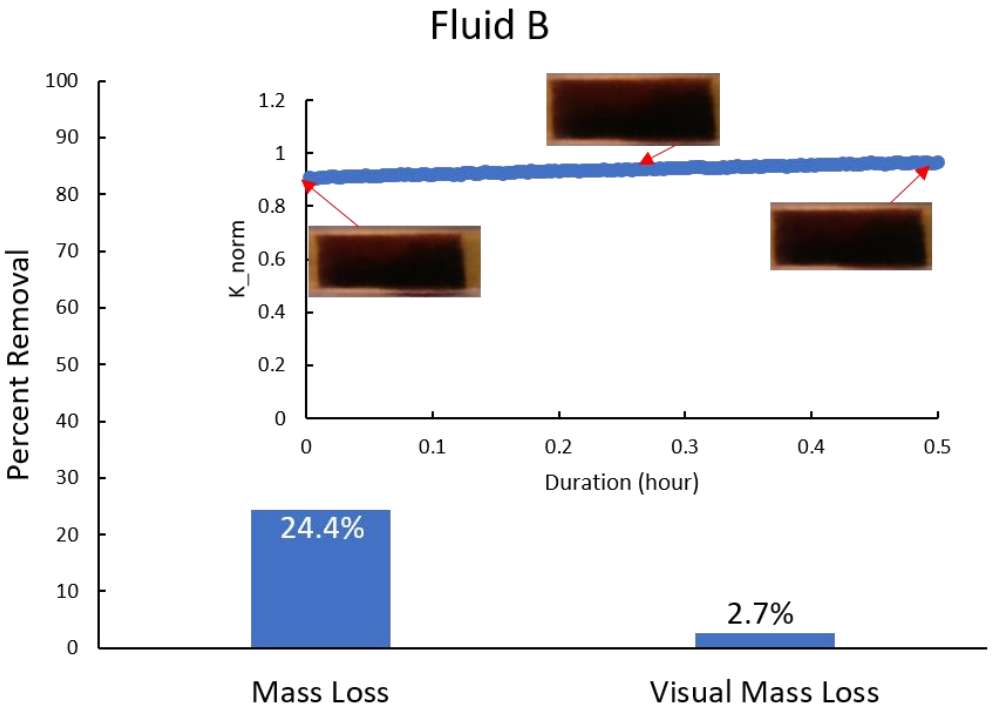

Figure 3-4: End of test varnish removal comparison between mass loss and visual mass loss data for fluid C. Inset graph shows normalized K data versus time with images of the coupon at time 0, 15, 30 minutes.

3.3 Temperature Dependence

The effect of temperature on varnish removal was tested with fluid A keeping the flow rate and cleaner concentration constant at 0.5 GPM and 20%, respectively. The temperature was varied from 60°C to 100°C with an interval of 10°C. For each test, the coupons were inspected at the beginning and the end of testing for removal characteristics. Particle analysis was performed to study the correlation between temperature and particle size. Visual data was processed for real time varnish removal.

As shown in Figure 3-5, the removal patterns are similar at all temperatures. The 100°C coupon and the 80°C coupon had the largest varnish overflow, meaning this varnish was outside the flow channel of the test region and was not exposed to consistent flow. By visual inspection of the posttest coupons, the high-temperature tests failed to remove as much varnish as the low-temperature tests. The remaining varnish is primarily at the inlet side of the coupon (top of the images). This is confirmed by the data in Table 3-1, which shows that 10.3 mg of varnish remained on the coupon in the 100°C test while 3 to 5 mg remained for the lower temperature tests.

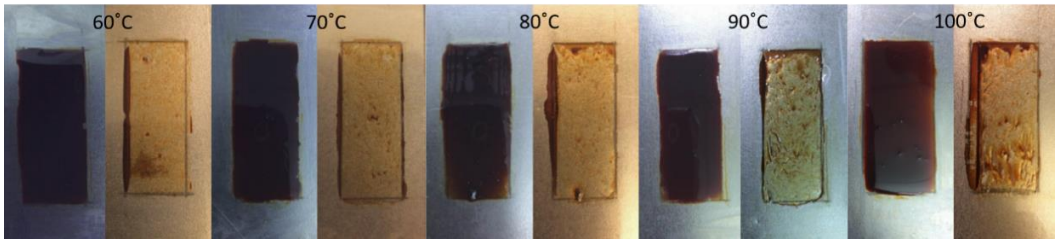

Figure 3-5: Test coupons at the beginning and end of testing. The flow direction for all tests coupons is from top to bottom on the page. The tests temperatures were varied from 60° C to 100°C with an interval of 10°C

Table 3-2: The Reynolds number and coupon weight before and after test for each temperature tested.

Temperature (°C)	Reynolds Number	Pre-test weight (mg)	Post-test weight (mg)
60	154.0	98.3	3.8
70	213.7	76.7	3.4
80	285.5	83.8	4.4
90	369.6	80.2	5.7
100	370.6	74.7	10.3

Visual inspection of the filters did not reveal a significant trend in particle size with temperature, as shown in Figure 3-6. The size of the particles on the filters was also analyzed from the digital data, and it was found that the average particle size in these tests was 567μm +/- 59.8μm and there was no statistically significant variation in average size with temperature.

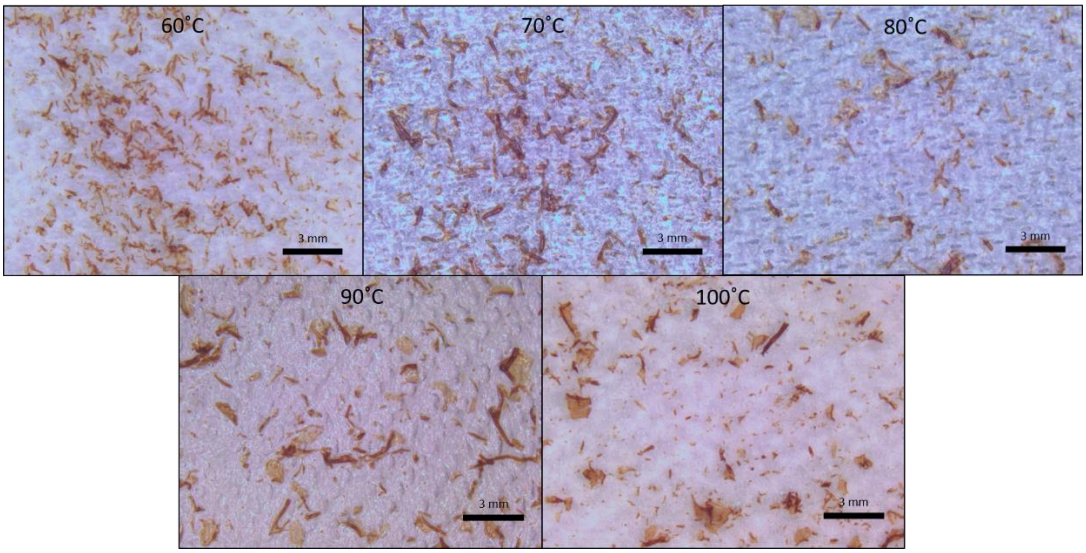

Figure 3-6: Optical microscope images of the posttest 5 µm filters with accumulated varnish particles at 10x magnification.

The number and root mean square size of the particles is shown in Figure 3-7. The average size of particles counted from each filter image showed no significant trend with temperature. The number of particles decreased with temperature from 550 to 350. This should indicate the particle size is increasing but data is inconclusive.

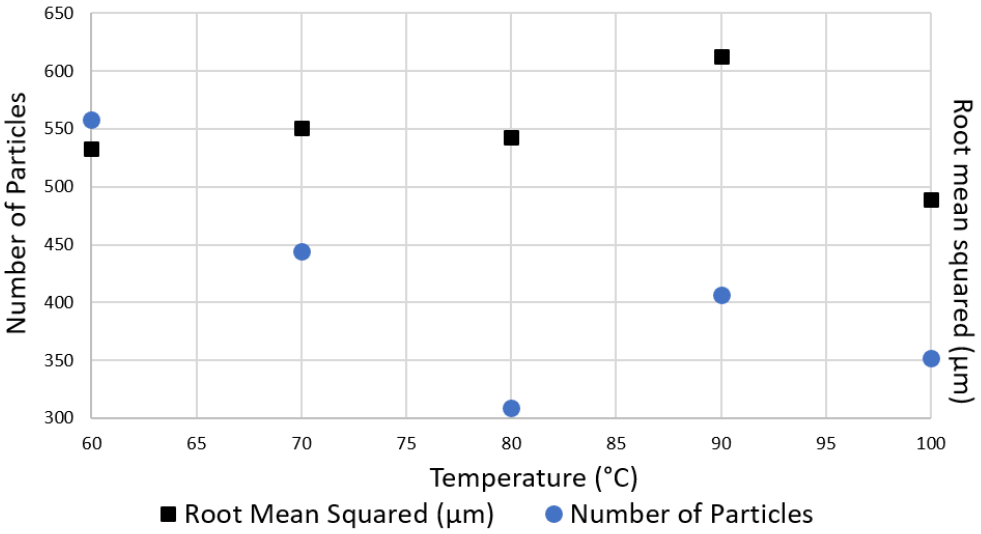

Figure 3-7: Number of particles (left y-axis, blue circles) and root mean square size of the particles (right y-axis, black squares) as a function of temperature. The concentration was 20% and the flow rate was 0.5 GPM for all tests.

Figure 3-8 shows that the rate of removal increases with temperature. There is a significant increase in removal rate as the temperature increases from 60 to 70°C, and then again from 90 to 100°C. Increasing temperature increases the diffusion of solvent into the varnish and softens the varnish. The varnish softening is caused by increased degrees of freedom on the polymer backbone. The added degrees of freedom lower the density of the polymer and decrease its mechanical strength (Equation 1-2). With more diffusion, new sites on the varnish chain are possible for scission. Together, these factors will cause more varnish to be removed at higher temperatures.

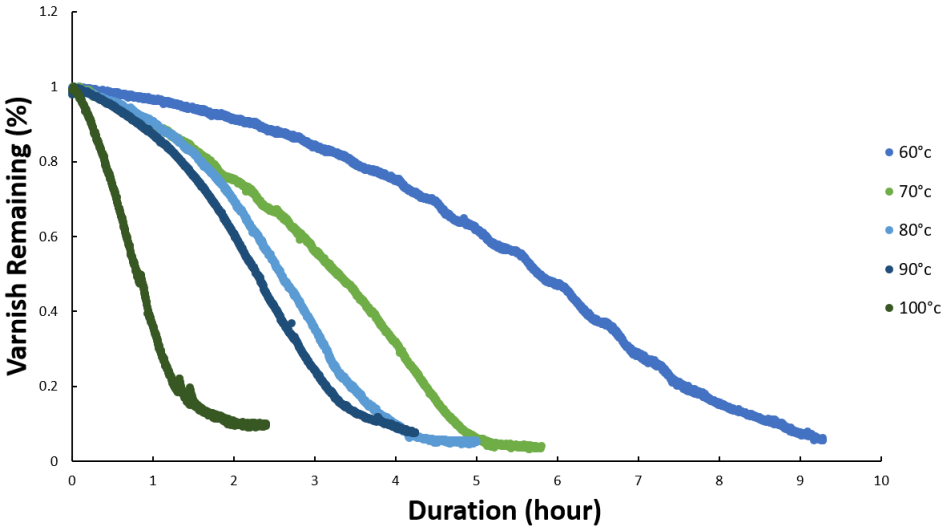

Figure 3-8: Varnish removal at 60°C, 70°C, 80°C, 90°C, 100°C. For each of these tests the concentration and flow rate were held constant at 20% and 0.5 GPM, respectively.

The relationship between removal rate and temperature is illustrated in Figure 3-9. This reinforces the observed effect that the removal rate decreases with temperature. The relationship between the removal at 10% and 90% follows a 3rd order polynomial trend. One key observation from this is that the most significant change in removal rate occurs between 60 and 70° C. Therefore, this cleaner can be used to remove varnish efficiently at temperatures higher 70° C or higher.

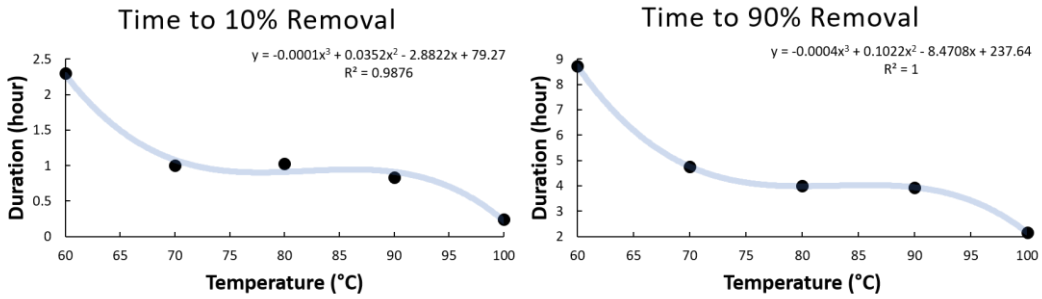

Figure 3-9: Time required to remove 10% (left plot) and 90% (right plot) of the varnish as a function of temperature. The symbols represent measured data and the lines are polynomial fits to the equation. The fit equations and R squared values for the fits are shown in the plots.

3.4 Flow Dependence

The effect of flow rate on varnish removal was tested in a series of tests. The temperature and cleaner concentration were held constant for all tests at 90°C and 20%, respectively. The flow

rates were tested at 0.1, 0.5, 1.0, 1.5, 2.0, and 4.0 GPM. These flow rates are relevant to lubricant flow in many mechanical components.

The removal patterns are consistent throughout all flow rates, as shown in Figure 3-10. The final removal is visually equivalent at all flow rates tested, with a slight trend towards more removal above 2.0 GPM. This is supported by the mass removal data shown in Table 3-2. There is very little residual varnish at the inlet after removal has reached steady state.

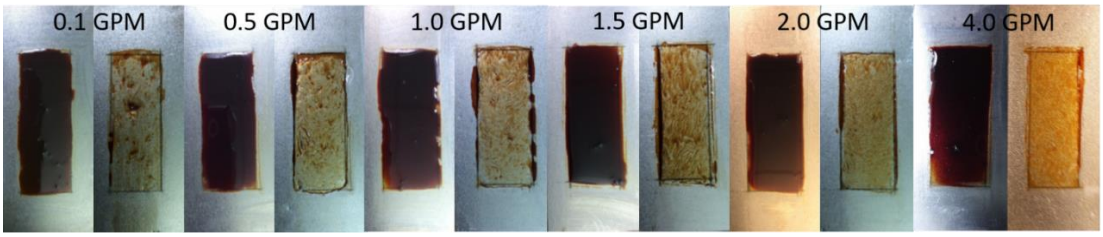

Figure 3-10: Test coupons at the beginning and end of testing. The flow direction for all tests coupons is from top to bottom on the page.

Table 3-3: The coupon weight before and after test for each flow rate tested.

Flow Rate (GPM)	Reynolds number	Pre-test weight (mg)	Post-test weight (mg)
0.1	73.9	83.1	9.2
0.5	369.6	80.2	5.7
1.0	739.2	82.4	7.8
1.5	1108.8	82.2	8.0
2.0	1478.4	83.0	5.5
4.0	2956.7	84.9	3.4

Visual inspection of the filters (Figure 3-11) shows a correlation between particle size and flow rate. Large particles are seen at 0.5 gallons per minute and consistently reduce in size with each increase in flow. There is a deviation in this trend at 0.1 gallons per minute. The deposition of particles for the 0.1 GPM sample was not consistent because the flow did not properly seat the filter to the filter housing and particles flowed around the filter cloth.

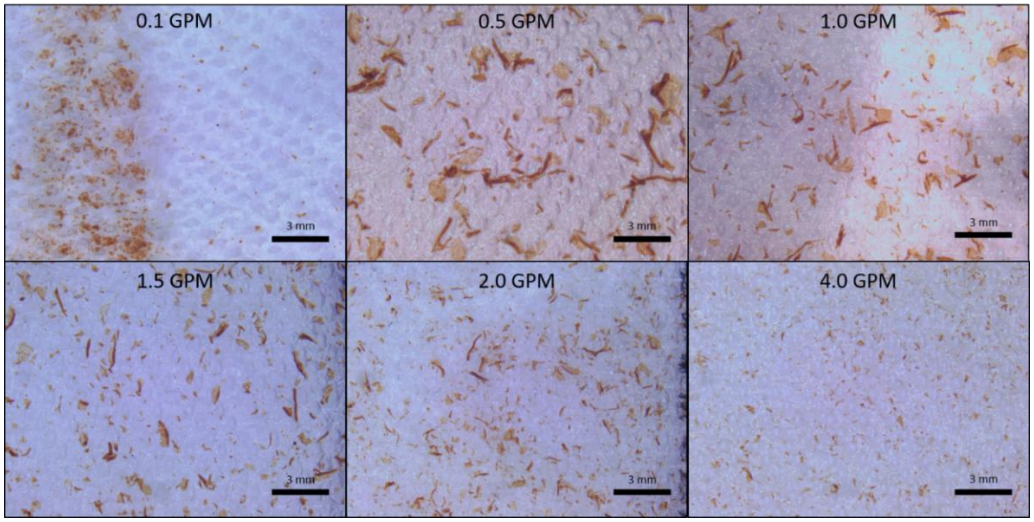

Figure 3-11: Post-test images of the 5 µm downstream filter at 10 times magnification.

The particle size results are analyzed quantitatively in Figure 3-12. With the exception of the slowest flow rate, where the filter did not seat correctly, the size of the particles decreased, and the number of particles increased with increasing flow rate. This illustrates that, as portions of the varnish are softened and begin to detach from the surface, the material is removed more quickly with higher shear rates which decreases the size of the particles captured in the filter. This observation is supported by the fact that particle number increases as the average particle size decreases. In general, smaller particles are preferred because the chance of downstream clogging is reduced. This would indicate that running this cleaner at a high shear rate would be preferable. However, in some systems, filtering of particles is preferable as opposed to hot draining the system. In these instances, a lower shear rate would be preferable.

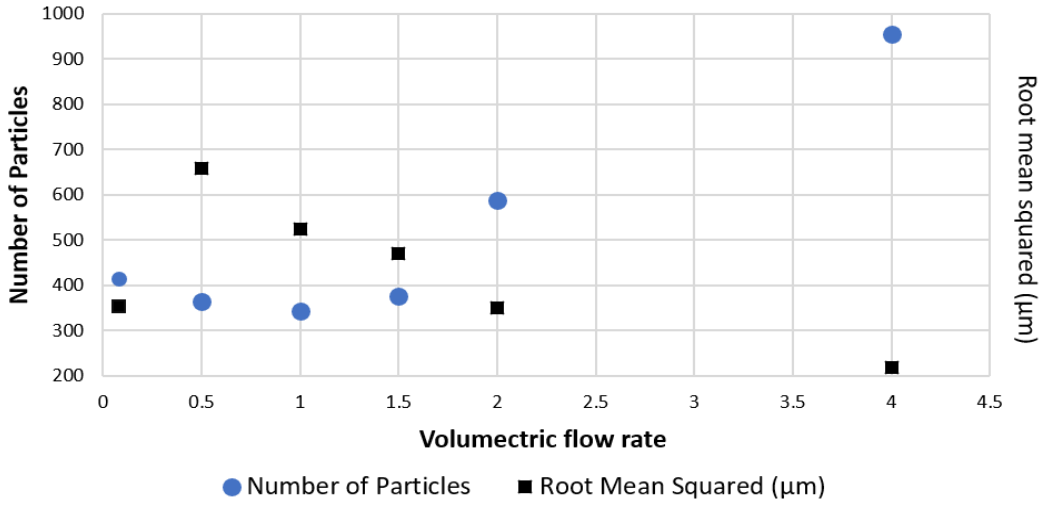

Figure 3-12: Number of particles (left y-axis, blue circles) and root mean square size of the particles (right y-axis, black squares) as a function of flow rate. The concentration was 20% and the temperature was 90° C for all tests.

The effect of flow rate on varnish removal is shown in Figure 3-13 which shows that varnish is removed faster at higher flow rates. The time to 10 and 90% removal is shown in Figure 3-14. These results show that the time required for varnish removal decreases rapidly with flow rate. The data was fit to a power law equation and the fit lines are shown in Figure 3-14. These results indicate that higher flow rates are preferred for removing varnish rapidly, but that it may not be necessary to run the system at higher than 2 GPM, since the difference between removal time at 2 and 4 GPM was relatively small.

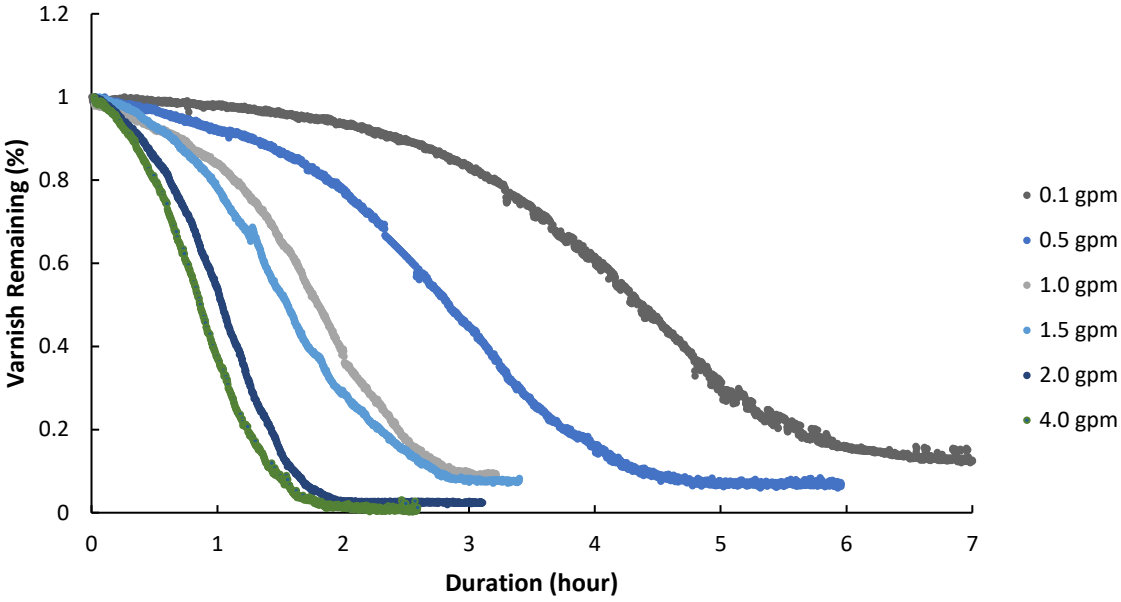

Figure 3-13: Percent of varnish remaining on the coupon versus duration of test for all flow rates ranging from 0.1 GPM to 4 GPM. The concentration was 20% and the temperature was 90° C for all tests.

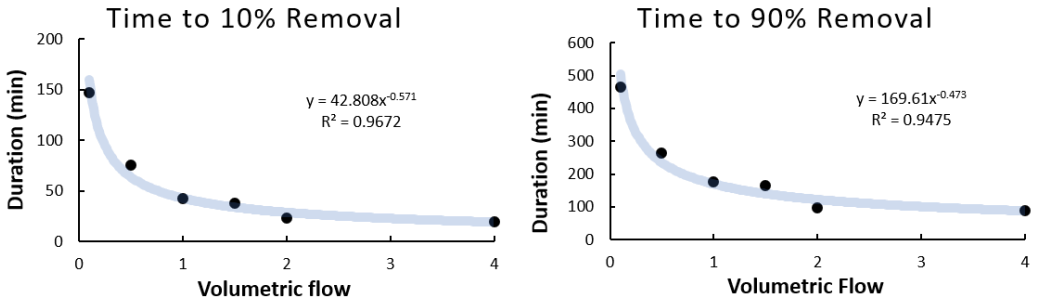

Figure 3-14: Time required to remove 10% (left plot) and 90% (right plot) of the varnish as a function of flow rate. The symbols represent measured data and the lines are power law fits to the equation. The fit equations and R squared values for the fits are shown in the plots.

The primary effect of differing flow rates on varnish removal is due to its impact on the shear forces at the surface of the varnish. The increase in shear force allows the chemical cleaner to remove the particles at an earlier stage in their degradation from the bulk varnish on the coupon. This results in decreased particle size and an increase in removal rate.

An interesting phenomenon was observed in the direction of varnish removal that may be correlated to the flow rate. Figure 3-15 shows all the flow test coupons at 50% removal, which shows that removal begins at the downstream edge of the varnish moving forward for all the coupons at or below 1.0 GPM. The removal for 1.5 and 4 GPM is from the front end of the varnish to the back. 2.0 GPM removal is from the back end of the varnish forward. This phenomenon may be caused by the flow rate or by inconsistencies in the surface geometry of the varnish.

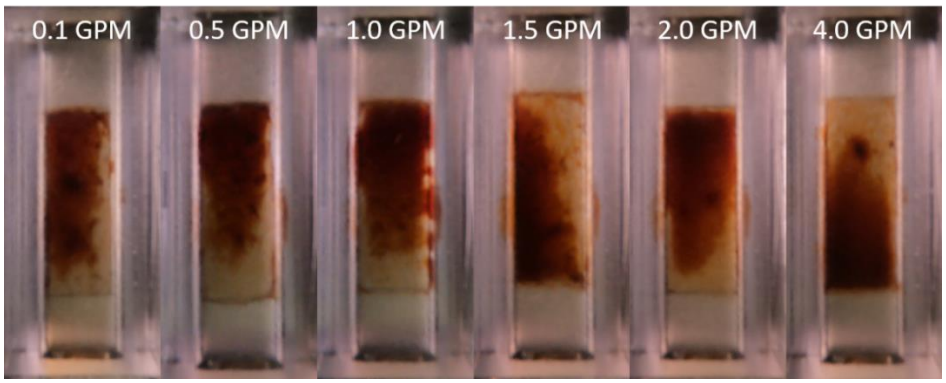

Figure 3-15: Images of varnish removal at 50% removal for all flow tests. The flow direction is from the top of the image down and shows the direction of removal.

3.5 Concentration Dependence

The effect of concentration on varnish removal was tested using the chemical cleaner mixed with base oil at 5%, 10%, 15% and 20% concentrations. The temperature and flow rate were kept constant at 90°C and 0.5 GPM, respectively, for all tests. The range of concentrations tested is reasonable for typical chemical cleaners in the gas turbine industry. Many of the cleaning additives are volatile and bring down the flash point of the oil. Higher cleaning additive concentrations could be dangerous in operation. Therefore, it is desirable to use the minimum amount of cleaner to effectively remove the varnish. Images of the coupons in Figure 3-16 show that, as expected, higher concentrations remove more varnish. This is also observed in Table 3-4 which shows that the least varnish remained on the coupon at the highest concentration.

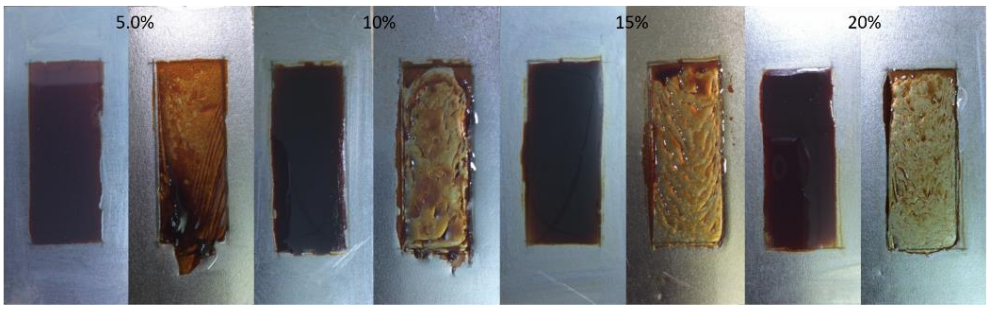

Figure 3-16: The test coupons at the beginning and end of testing. The flow direction for all tests coupons is from top to bottom of the page.

Table 3-4: The coupon weight before and after test for each concentration tested.

Concentration (%)	Reynolds number	Pre-test weight (mg)	Post-test weight (mg)
5.0	372.7	72.7	28.0
10	371.7	89.2	19.8
15	370.6	88.1	8.7
20	369.6	80.2	5.7

The removal characteristics vary greatly between chemical concentrations, as shown in the images of the particles on the filter in Figure 3-17. The 5% percent concentration fluid softens the varnish and allows it to elongate in the direction of flow but there is no indication of large particle removal. The 10 and 15% percent concentration fluids have evidence of large particle removal accompanied with an increase in end-of-test removal. The large particles indicate that increased shear forces were needed to detach the particles from the surface of the varnish indicating the mechanical strength of the varnish was still high. The 20% concentration fluid has a smaller particle removal characteristic with the highest level of end-of-test removal.

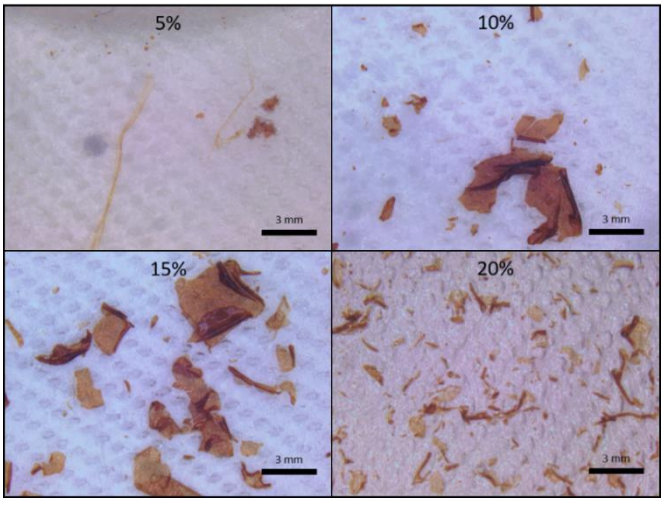

Figure 3-17: Post-test image of the 5 µm downstream filter at 10 times magnification.

The digital particle data shown in Figure 3-18 does not exhibit a decisive trend. The number of particles increases very slightly with concentration up to the maximum concentration of 20%. We can see that size of the particles increases dramatically up to 15% but then decreases at 20%. However, it was very difficult to get a viable sample space to represent the entire filter with this sparse distribution of large particles, so the particle count and size trends may not be statistically significant.

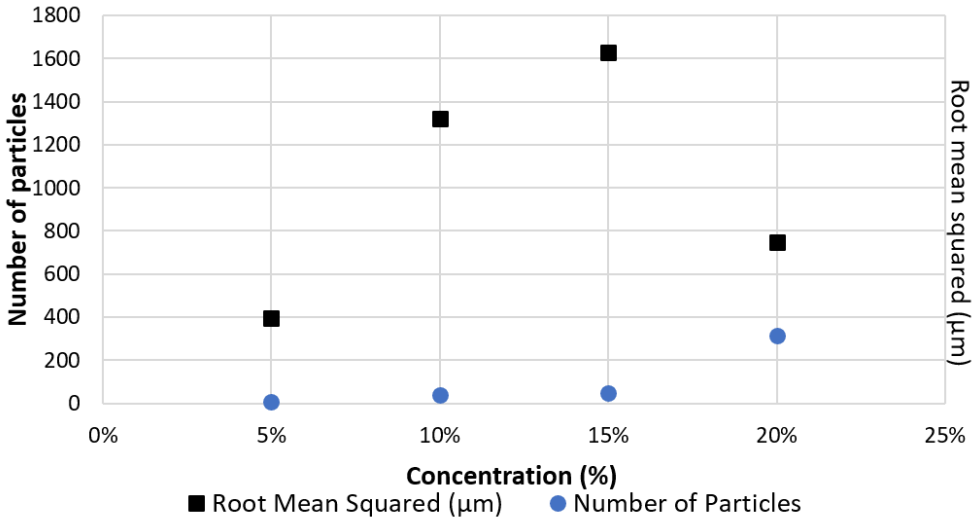

Figure 3-18: Number of particles (left y-axis, blue circles) and root mean square size of the particles (right y-axis, black squares) as a function of concentration. The flow was 0.5 GPM and the temperature was 90° C for all tests.

Figure 3-19 shows that the concentration of cleaner has a large effect on removal time. The difference between steady-state removal from 5% to 10% concentration is 110 hours. The 5% concentration could only remove 60% of the varnish present on the coupon and did not begin removing varnish until after 30 hours. The 10% concentration took eight hours to initiate the removal process and reached steady state at 80% removal. The 15 and 20% concentrations have very similar removal curves with 15% needing 45 minutes longer to engage the removal process. The relationship between concentration and varnish removal is illustrated in Figure 3-20. This relationship is governed by a power function with a diminishing effect on removal rate as concentration is increased. This points to a threshold concentration for efficient removal and that increasing the concentration above this threshold does not significantly increase varnish removal. In many applications the concentration should be kept to a minimum to increase the lubricity of the cleaning fluid as it is circulated through the lubrication system and reduce issues with flash point.

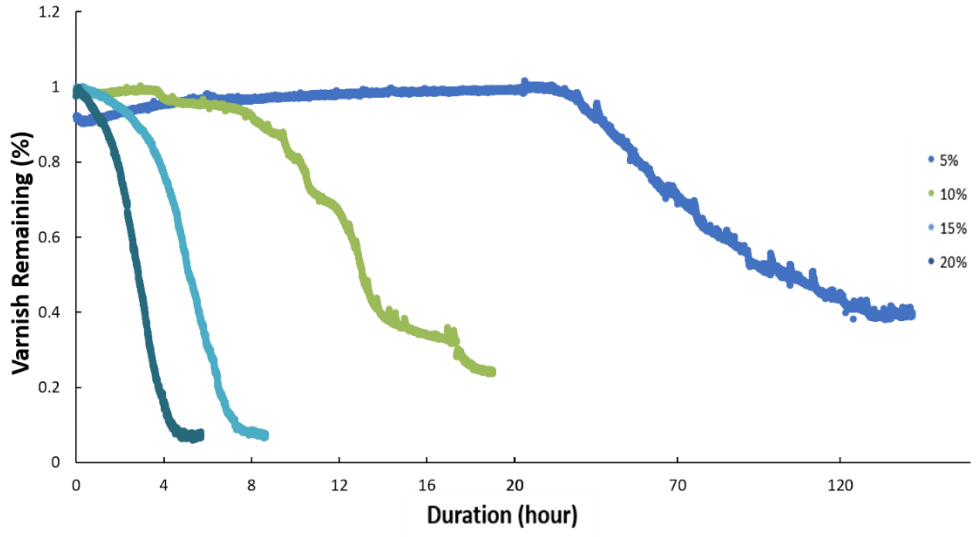

Figure 3-19: Percent of varnish remaining on the coupon versus duration of test for all concentrations ranging from 5% to20%. The concentration was 20% and the temperature was 90° C for all tests.

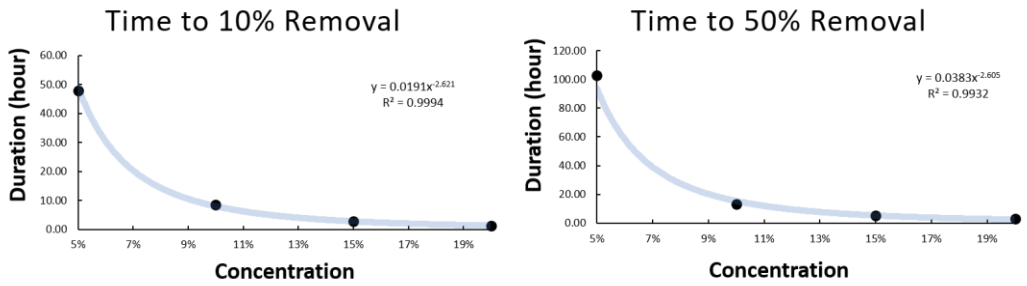

Figure 3-20: Time required to remove 10% (left plot) and 50% (right plot) of the varnish as a function of concentration. The symbols represent measured data and the lines are power law fits to the equation. The fit equations and R squared values for the fits are shown in the plots.

3.6 Fluid Flow Analysis

The above testing showed that varnish can be removed most effectively at high temperatures and shear rates, as well as with larger concentrations of chemical cleaners. The concentration and temperature effects are straightforward, since more chemical cleaner and hotter temperatures will soften and reduce the molecular weight of the varnish allowing for accelerated removal. However, to better understand the shear rate effects, a computational fluid dynamics analysis was performed. In the first series of tests a 2D test cell was generated and the shear rate was calculated at the leading and trailing edges of the varnish as shown in

Figure 3-21. The shear rates were calculated for each flow rate tested in the experiments to visualize trends correlated to flow velocity. A second series of tests was performed by slightly changing the geometry of the varnish. In one series, the varnish was tilted forward into the flow and in the second series the varnish was tilted backward away from the flow, as shown in Figure 3-22. The shear rates were calculated at the leading and trailing points for all tests and compared to better understand the effect of geometric features on the surface of the varnish.

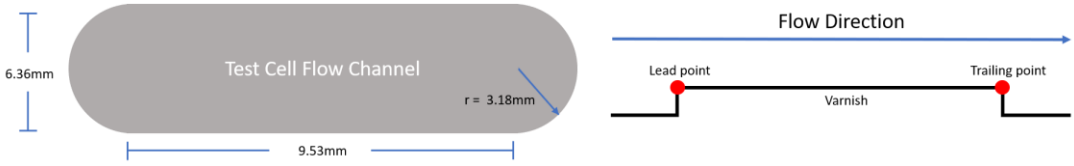

Figure 3-21: Left, the flow cell test channel with dimensions; right, the flow direction over the varnish surface with indications of the points of calculation of shear rate at the leading and trailing edges of the varnish.

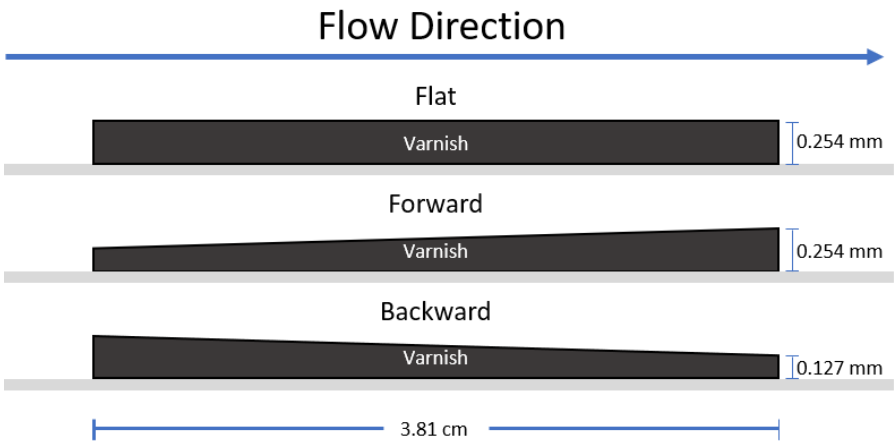

Figure 3-22: Varnish profiles used in flow simulations. The flow direction is from the left to the right. A simulation of all flow rates was performed for each profile.

3.6.1 Model

The simulations were performed using COMSOL multi-physics. A 2D flow channel was developed with a length of 80 mm and a height of 6.36 mm. At the center of the bottom surface of the flow channel, a portion of the wall was inset to simulate the varnish. The in-plane dimensions of the varnish were 38.1 mm x 256 µm. The geometry of the varnish was varied to present an inclined face and declined face to the flow (Figure 3-22). All the flow tests were performed with fluid A at 20% concentration and 90° C. Under these conditions, fluid A has a density of 869.09 kg/m^3 and a dynamic viscosity of 7.608 mPa*s. These values were used throughout all the tests as the material properties in the flow channel. These tests were performed in the laminar regime. All

flow rates used in the experiments corresponded to Reynolds numbers below 2000, except for 4 GPM which is slightly into the mixed regime but was approximated as laminar in these simulations.

The boundary conditions for the top and bottom walls, including the varnish inset, were set at zero-slip. At the inlet, a flow field was introduced assuming a circular flow channel. In this analysis we are only looking at the center line of the varnish and a circular geometry will not significantly affect the flow field at this point. The equation for the inlet flow velocity is the following:

$$u(h) = 2V_{avg}(1 - \frac{h^2}{H^2}) \qquad 3\text{-}1$$

In this equation, $u(h)$ is the fluid velocity at a given height (h) and (H) is the total height of the channel. The initial pressure at the inlet was set to 38 psi, as measured from experiments. The average velocity V_{avg} was set to the velocity calculated for each test by dividing the volumetric flow rate by the area of the test channel, 92.38mm^2. A summary of the flow rates and velocities are given in Table 3-5.

Table 3-5: List of velocities used for each test series

Name	Volumetric flow	Velocity (avg)
V_1	0.1 GPM	0.068412 m/s
V_2	0.5 GPM	0.34206 m/s
V_3	1.0 GPM	0.68412 m/s
V_4	1.5GPM	1.0262 m/s
V_5	2.0 GPM	1.3682 m/s
V_6	4.0 GPM	2.7365 m/s

The outlet was set at laminar flow with an exit pressure of 37 psi and an exit length of 0.2 m. The governing equations for this simulation are the conservation of momentum, Navier-Stokes and the continuity equation[34]. This application mode defines and solves the Navier-Stokes equations when density is constant. This is a steady-state simulation, so the derivative with respect to time is not included in the Navier-Stokes solution.

$$\rho(u \cdot \nabla)u = \nabla \cdot [-pl + \mu(\nabla u + (\nabla u)^T)] + F \qquad 3\text{-}2$$

$$\rho\nabla \cdot (\mathrm{u}) = 0 \qquad 3\text{-}3$$

$$u(0) = u(H) = 0 \qquad 3\text{-}4$$

3.6.2 Results

Pressure contour plots for each varnish geometry at a flow rate of 0.5 GPM and temperature of 90°C are shown in Figure 3-23. A slight gradient is observed across the test cell, as expected due to the viscosity of the oil and is a result of the fictional forces between fluid molecules. The

pressure contours at the leading and trailing edge of the varnish are symmetrical with a slight difference in pressures due to the gradient across the cell. The pressure gradient is consistent for all three geometries. This is expected considering the difference in geometry is small compared to the overall flow channel. The pressure contours at the leading and trailing edges of the varnish change with geometry slightly but the overall gradient remains constant.

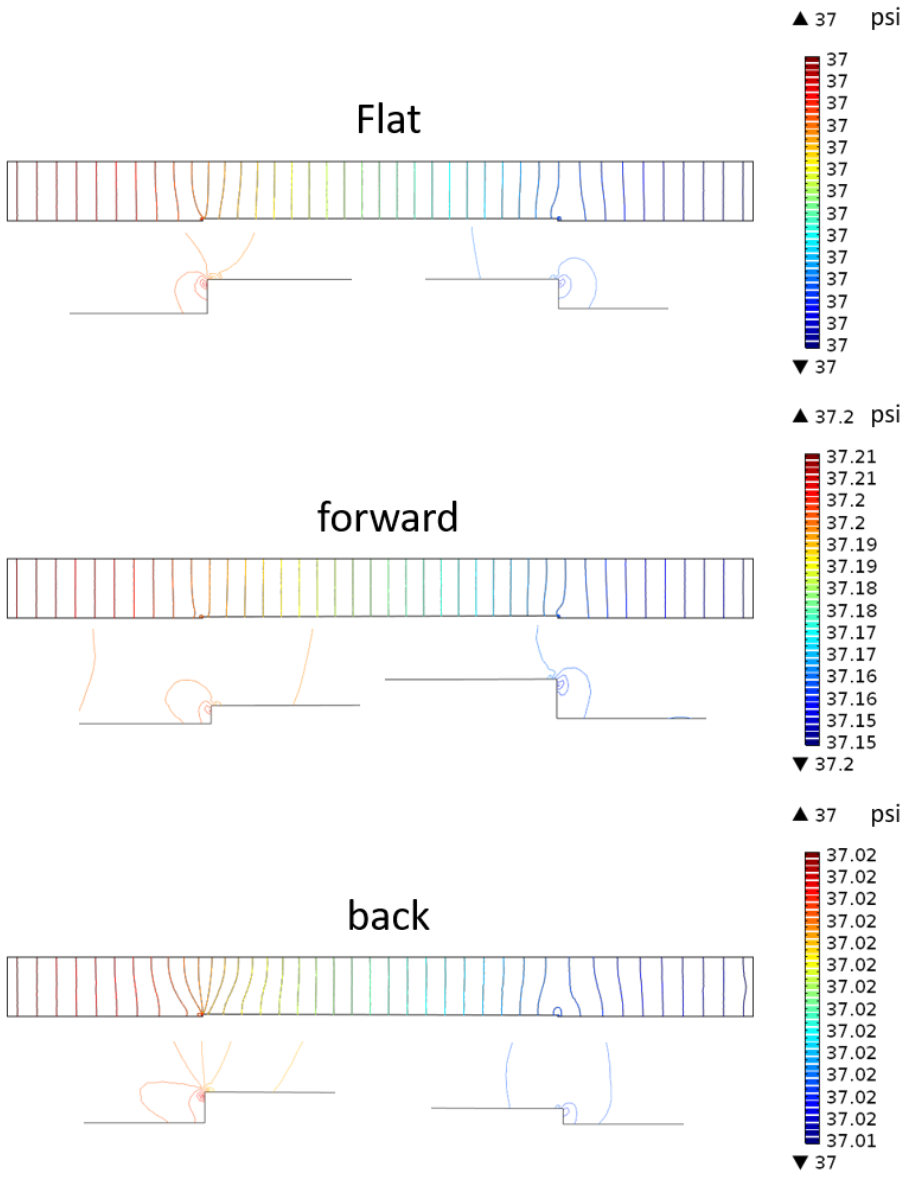

Figure 3-23: Contour plots of the pressure gradient (psi) with a zoomed in section of the leading and trailing edges of the varnish. Plot was generated for a 0.5 GPM. Top – flat geometry; Middle – forward geometry; Bottom – backward geometry.

The velocity fields at 0.5 GPM and 90°C are shown in Figure 3-24. The velocity contour plots show that, at the no slip boundary, there is zero velocity and the highest velocity is at the center of the flow channel. The average velocity is consistent with experimental inputs. As expected, there is a velocity increase when the flow encounters the constricted region above the varnish. Due to the laminar flow regime of this test, there is no mixing occurring at the sharp edges of the varnish.

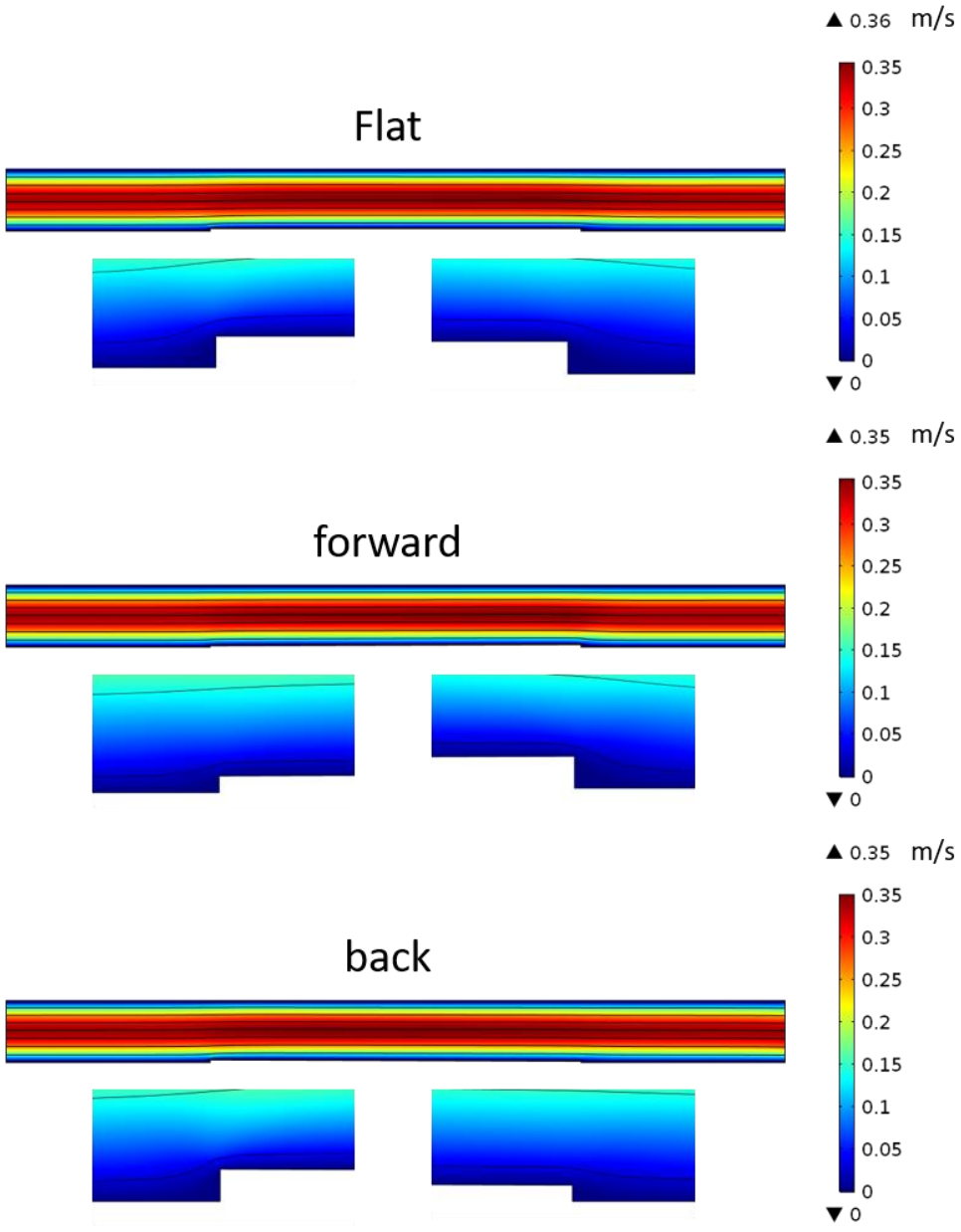

Figure 3-24: Velocity magnitude plot (m/s) with streamlines overlaid. Plot was generated for 0.5 GPM. Top – flat geometry; Middle – forward geometry; Bottom – backward geometry.

Varnish is a polarized hydrocarbon that polymerizes on metal surfaces. This polymerization is not homogeneous across the surface of the varnish and will create features that can induce areas of high and low shear rate. If we compare the forward and backward simulations with the flat simulation, we see that different geometries can induce a higher shear rate, thereby increasing the potential removal rate. This difference is analyzed quantitatively next.

The shear rate was calculated at the leading edge and trailing edge of the varnish for all six flow rates tested in the experiments. The shear rate at the leading edge is shown in Figure 3-25. As expected, the shear rate increases with flow rate. Also, the shear rate is lowest for the forward geometry at any flow rate. This can be explained by the bottlenecking effect on fluids entering a restricted region. The smaller step at the beginning of the varnish allows for a more gradual acceleration of the fluid.

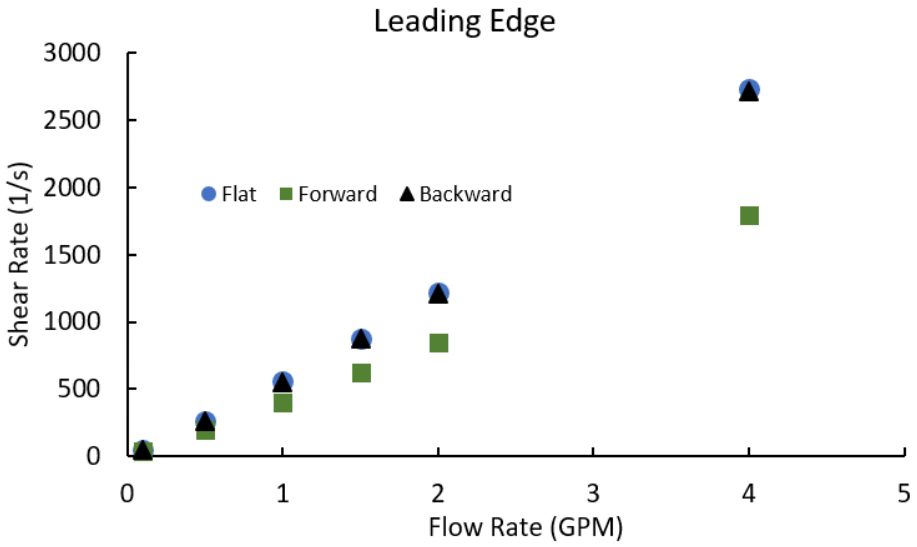

Figure 3-25: Shear rate at the leading edge of the varnish versus the volumetric flow rate for all three geometries.

The shear rate at the training edge of the varnish is shown in Figure 3-26. At the trailing edge of the varnish, the backward facing geometry has a lower shear rate increase with volumetric flow than the forward-facing geometry or the flat geometry. The larger shear rate of the backward geometry increase the overall varnish removal rate, but the effect is likely to be small.

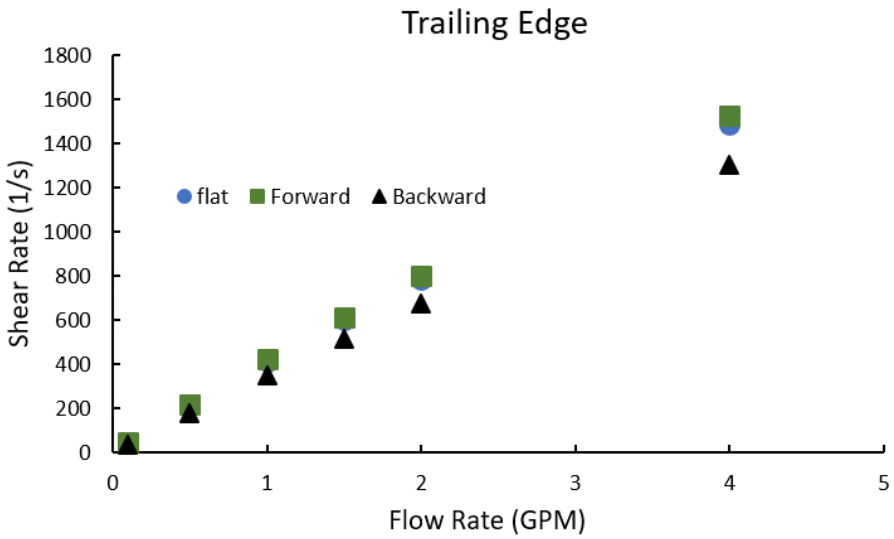

Figure 3-26: Shear rate at the trailing edge of the varnish versus flow rate for all three geometries.

The difference between the shear rates at the leading and trailing edge was calculated. From Figure 3-27 we can see that the forward geometry has a negative difference for 0.1, 0.5 and 1.0 GPM. This indicates that the shear rate, and therefore shear stress, is higher at the trailing end of the varnish and could induce removal from the downstream edge of the varnish forward. This should only occur if the flow rate is at or below 1.0 GPM and a forward-facing geometry is present in the varnish. This phenomenon was observed in experiments when flow rates were below 1.0 GPM as seen in Figure 3-15. For the other geometries and for higher flow rates, the shear rate difference is negative. This indicates that varnish should be removed first from the upstream edge of the varnish. This is observed in experiments with some exceptions at faster flow rates as shown in Figure 3-15.

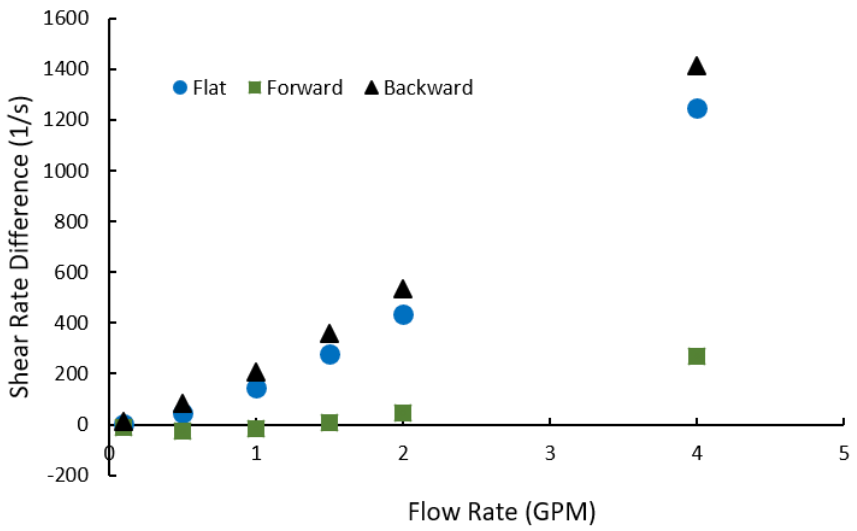

Figure 3-27: The difference between the shear rate at the leading edge and at the trailing edge of the varnish versus flow rate for all three geometries.

A second set of simulations were run using the flat geometry at varying temperatures to determine if the fluid contributes to the observed effect of temperature on varnish removal. For these calculations, the density and viscosity of the fluid were calculated at each temperature and used as material properties, reported in Table 3–6. These tests were run at 0.5 GPM, consistent with experimental tests at varying temperatures.

Table 3-6: Density and viscosity of the viscosity for simulations at 0.5 GPM.

Temperature (°C)	Density (kg/m^3)	Viscosity (Pa*s)
60	886.1	0.0186
70	881.3	0.0133
80	874.4	0.0010
90	869.1	0.0076
100	860.7	0.0060

Figure 3-28 shows the shear rate at the leading edge, center and training edge of the varnish as a function of temperature. We observed that the shear rate increases with temperature at the leading edge of the varnish and decreases with temperature at the trailing edge. The shear rate at the center of the varnish remains constant at all temperatures. The average shear rate for the three points increases only by 0.8% over the 40°C temperature increase. This is not consistent with the large change in varnish removal rate with temperature observed in the experiments. Therefore, the temperature effect is likely due to changes to the varnish, i.e. softening, as opposed to effects of the fluid that cause changes in shear stress on the varnish.

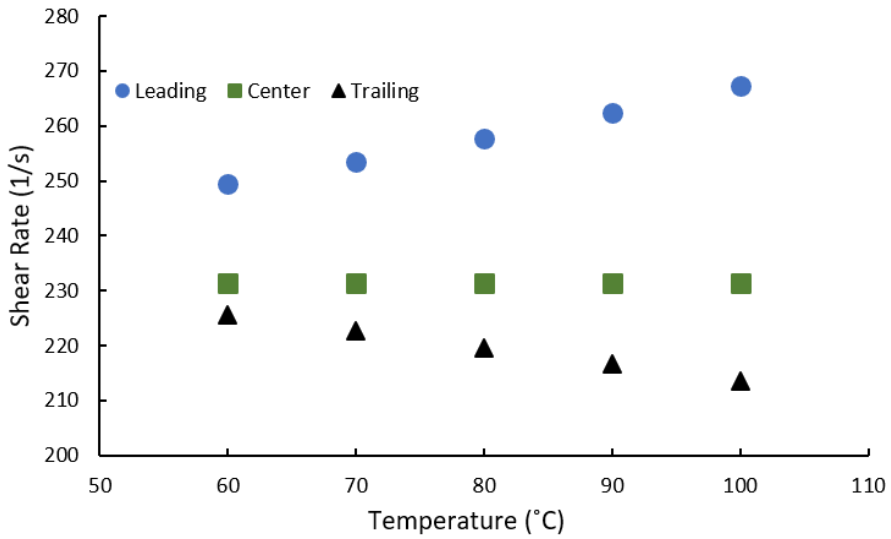

Figure 2-28: Shear rate at the leading, center and trailing edge of the varnish at all temperatures tested.

4 Conclusion

4.1 Discussion of results

The commercial tests were a continuation of previous work [14] in developing a standardized procedure by which chemical cleaners can be measured. The tests performed in this research differed from the previous tests by the oxidation level of the varnish and the flow rate. The soft varnish used in this research had a higher residual monomer level allowing for more pliability. We tested these samples at a low flow rate, simulating larger flow channels and sump regions of the lubrication system. These tests indicated that very few chemical cleaners were capable of removing significant portions of varnish at low flow. Only two of the six fluids were successful in removing significant varnish. In the development of a standardized test for chemical cleaners, each fluid should be tested at a range of flow rates and temperatures to achieve a complete picture of removal properties for comparison.

The long tests that were run with commercial fluids that did not remove significant varnish brought to light a drawback to the visual analysis process. As shown in Figure 3-4, the varnish darkened in the early stages of mechanochemical removal. This was not an issue in the past due to the high flow rate and oxidation level of the varnish tested. The soft varnish in this series was semitransparent at the beginning of the test, allowing for the chemical surface effect to diminish accuracy. The transparency of the varnish led to three primary issues. The first issue was that the soft varnish formulation was much lighter in color and transparence than higher oxidative level varnish tested before. The second issue was the distribution of mass was not homogeneous over the coupon surface, allowing for areas of high transparency. The third issue was that the chemical texturing of the surface of the varnish diffracted light and increased the

average K value of the image. We could address this issue going forward by increasing the average mass of the varnish on the coupon could be increased from 80 mg to 100mg and taking measures to ensure that the varnish distribution is homogeneous. These steps will not completely eliminate the problem if the test does not remove significant varnish. The texturing of the surface will darken the varnish even if the coupon is not visible through it. This will artificially mask removal at the beginning of each test. Although this is a drawback, the maximum varnish removal that was masked by this effect was 21.7% and this number could be reduced using the above-mention steps. Therefore, for an industrial classification, the test method is still a valuable indicator of the efficiency of varnish removal.

The extensive tests performed with fluid A illustrated significant trends dependent on temperature, flow rate and chemical concentration. These distinctive trends can be used to predict the behavior of fluid A in different regions of a lubrication system. A second benefit to this research is the active formulation and testing of a removal fluid to increase its effectiveness. We have been able to test and produce data integral to the formulation of chemical cleaners more effective over a larger range of working conditions.

Analysis of particle data obtained from filter images using methods developed in this study provides a useful added metric for comparing chemical cleaners. This data was primarily useful in establishing a strong correlation between flow rate and particle size. The temperature and chemical concentration tests were less conclusive, showing slight inconsistences in the relationship between number of particles and the root mean squared of the particles. This may be due to a lack of sample size and conformity of the particle distribution on the filter. The sample size was mitigated by taking three pictures of each filter to increase sample size. The problem of filter fluid bypass at low flow rates continues to be an issue. This problem may need a redesign of the filter housing to completely alleviate the bypass.

The computer simulations run shed light on features of removal observed in experiment. Removal overwhelmingly started from the leading edge of the varnish, but in some experiments, removal was observed starting from the trailing edge forward. These simulations showed that, if flow rate is low, the difference between shear rate at the leading end trailing end of the varnish is small and can be influenced by slight changes in thickness. These simulations supported the assumption that small geometric differences in the varnish surface will not greatly change the overall removal rate, only the removal rate at finite regions.

4.2 Future work

The results obtained in this research suggest two future research directions. First, improved accuracy might be achieved by developing a method to determine when varnish removal images are adversely affected by test cell lid degradation. Second, while this study focused on varnish removal, varnish issues can also be addressed by minimizing its formation in the first place. Future research can include development of an approach to measure varnish formation, as opposed to removal.

4.2.1 Optimization of varnish removal accuracy

Optical consistency is an important parameter for achieving consistent accuracy with this test method. The images are taken through a polycarbonate lid and 6.36 mm of cleaning fluid. Variations in the hue of the cleaning fluid is normalized out by the test operating procedure, but clarity of image can be affected by the degradation of the polycarbonate lid. As the polycarbonate lid degrades, the features imaged through the flow channel become less distinct as shown in Figure 4-1.

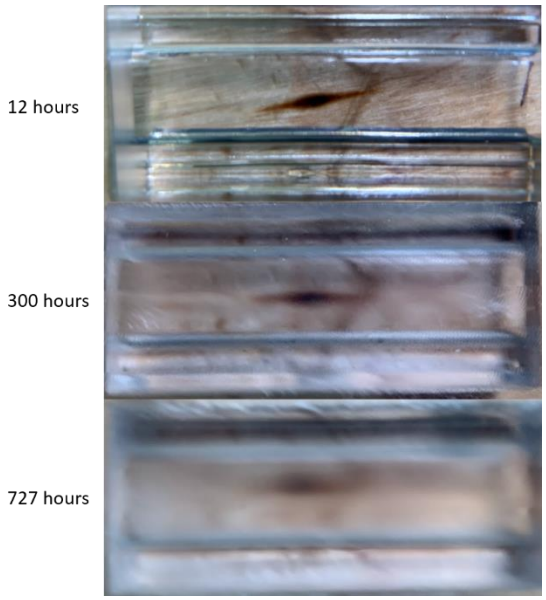

Figure 4-1: Degradation of polycarbonate lid illustrated from photos taken during a test at 12, 300 and 727 hours.

The temperature and chemistry of the chemical cleaner also play a role in the speed of degradation. The effect of lid degradation has not had a significant effect on the visual removal data's precision, but going forward, a criterion should be set for minimum optical clarity. The definition of resolution is the ability to distinguish between two points. A two-point dot test could be devised to distinguish the degradation at which these dots are indistinguishable from each other. To set the resolution threshold, standardized tests could be run using the lids at different stages of degradation, or obscure the image with successive layers of material, such as mat-scotch tape. The critical resolution of these tests could be determined as the point that the results started to diverge from the original standardized tests with the 12-hour lid. This may help ensure consistent data and reproducibility.

4.2.2 Characterizing varnish accumulation

Working together with our collaborators, we are in the preliminary stages of designing a varnish accumulation rig. This test rig will use visual data, similar to the varnish removal rig, to measure real time varnish accumulation. This new rig would be used to test a different style of varnish

mitigation. Oil additives such as antioxidants and diffusers allow oil to neutralize and to suspend varnish precursors, slowing or eliminating the formation of varnish. This rig would be employed in testing these additives and their effectiveness in varnish mitigation. The rig should have the ability to vary temperature and flow rate to test different mechanisms of varnish formation.

Varnish accumulation is a slow process that can take months or years for a significant layer to form. This presents a considerable problem when attempting to devise a testing apparatus with a reasonable test timeline. To speed this process up we are attempting to implement two approaches to accelerated varnish formation. One is a thermal gradient that will increase precipitation of varnish particles present in oxidized oil. The second is hot surface cooking, or coking of the oil, where the metal surface in contact with the oil is above the stability temperature of the oil and rapid oxidation occurs[35]. The varnish that forms from a thermal gradient usually occurs in the sump or regions of the lubrication system away from the combusting surfaces, and it is usually a thin yellowish varnish. The varnish that occurs from coking is a high molecular weight, dark brown varnish that can form very rapidly[36].

For proof of concept we have conducted two tests. The first tests the hot surface coking prosses. We designed an apparatus that could be inserted into a beaker. The thermal energy was provided by cartridge heaters installed in the apparatus to encourage varnish formation on its surface. This device was built out of low carbon steel. A crossbeam was constructed to sit just below the surface of the oil to allow for uniform flow at the hot surface. The flow was induced by a magnetic stir tab and convective effects. Images of the test apparatus are shown in Figure 4-2.

Figure 4-2: (Left) Proof of concept test apparatus operating in base oil at 90° C with magnetic stir inducing flow and a crossbeam just below the oil surface. (Right) Full test apparatus with wired heating cartridges submerged in 125 mL of degraded oil.

A conceptual simulation was also run to better understand the thermal gradient on the apparatus. This would give us a better estimate of where varnish would form. The input parameters were 100°C at each cartridge insert point and a 5 W flux in the submerged region of the apparatus. The simulation results are shown in Figure 4-3. This shows that the hottest regions are on the columns next to the crossbeam, but the temperature gradient is small once steady state is reached. Through the simulation, we concluded that we would see varnish formulation on the pillars first and later on the crossbeam after prolonged exposure.

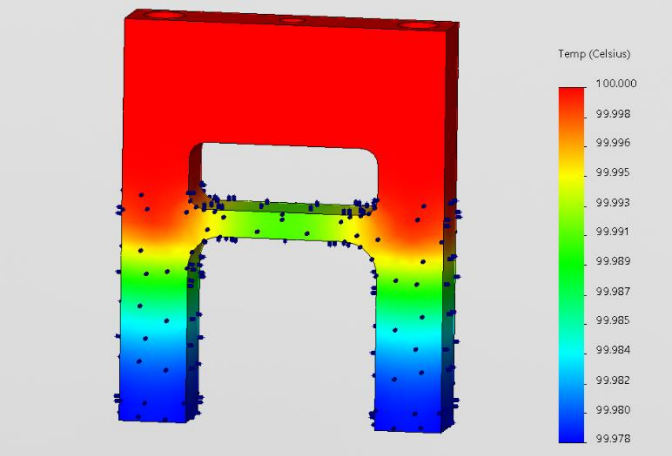

Figure 4-3: Temperature gradient of the varnish formation apparatus at 100°C at the cartridge inserts points with a 5 W flux below the oil level.

The proof of concept test was run at different temperatures ranging from 100°C to 250°C. Varnish formation was not observed until 200°C. The varnish formation on the apparatus occurred in an eight-hour test period, four hours at 200°C and four hours at 250°C. Most of the varnish was formed on the pillars at the hottest point of the insert. There was also a small amount of varnish formed on the crossbeam, as shown in Figure 4-4. This proof of concept test shows that we can produce varnish in a reasonable testing duration. With small alterations to this test rig we can allow for imaging of varnish formation at a hot surface.

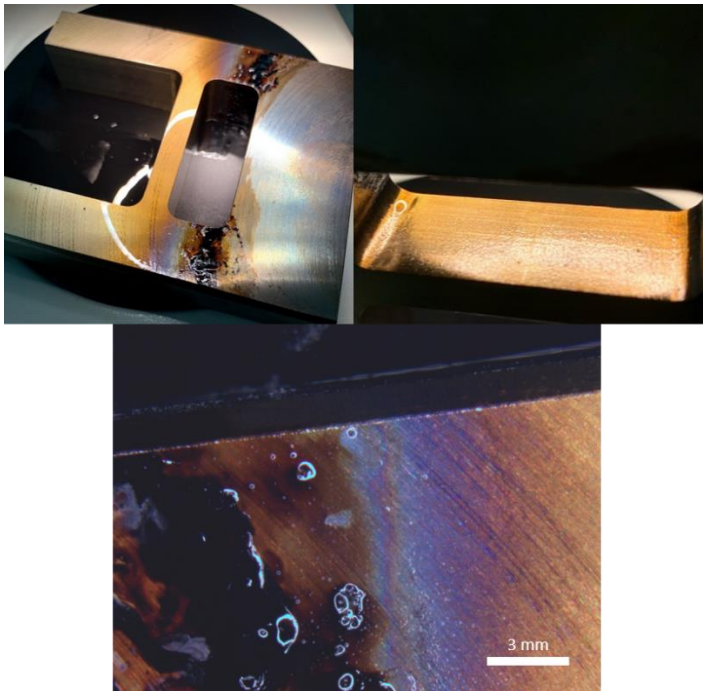

Figure 4-4: (Top left) Overall varnish formation primarily at side pillars at the surface of the oil. (Top right) Small varnish formation on the crossbeam. (Bottom) 10x magnification of varnish formed on the pillars.

The second proof of concept test explored thermal precipitation effects on suspended varnish particles. In this cold surface test, a cooled U-bend of steel was inserted into 300 mL of oxidized oil. The test rig is shown in Figure 4-5. The oil was heated by a hot plate to 100°C for one hour and then reduced to 60°C for one hour. The sequence was repeated in succession for the entire testing time. The steel U-bend was chilled to 0° C for the entirety of the testing. At this point, the proof of concept test has been run for over 40 hours with no appreciable varnish formation.

Figure 4-5: Thermal test set up, hot plate set at 100° C with magnetic stir simulating flow and 0° water circulating through the steel U-bend.

This work starts our team on the path to a new characterization tool for varnish mitigation. With this tool we can better understand additive control of varnish precursors in a circulating system. This new rig could not only help us better understand and compare existing additives but formulate more effective additives in the future.

4.3 Summary

Varnish is a cost of operating a mechanical system. Many mechanical systems reach very high temperatures; for example, gas turbine engines have areas of extreme temperature up to the 2000˚C [37]. This means that oxidation and oxidative byproducts are constant issues in these systems. There are many ways to mitigate varnish buildup and control oxidative byproducts, but chemical flushes are necessary if the varnish buildup reaches a critical point. This research investigated the effectiveness of different formulations of chemical cleaners in a standardized low-flow test and characterized the effects of flow, temperature and concentration on a single cleaner in a system. Overall, we ran 398 hours of commercial comparative testing. These tests allowed us to: (i) compare commercial cleaners at different operating conditions, (ii) refine the test procedure (iii) install upgrades for long-duration tests, and (iv) identify opportunities for future research. We also ran 329 hours of testing with fluid A, giving us a better understanding of the effect of operating conditions on varnish removal. Complementing these tests, comparative simulations helped us understand anomalies in the removal patterns of the varnish

at low flow rates and supported the assumption that the homogeneity of the varnish surface does not significantly affect removal rate. Overall, this study has provided a comprehensive characterization of varnish removal that will be useful in the industry to both formulate new cleaner fluids as well as identify optimal operating conditions for varnish removal.

References:

[1] L. R. Rudnick, Ed., *and Bio-Based Lubricants*. CRC Press Taylor & Francis Group, 2006.

[2] W. Holweger, "Fundamentals of Lubricants and Lubrication," *Tribology*, p. Ch. 1, 2013.

[3] P. L. Menezes, C. J. Reeves, and M. R. Lovell, *Tribology for Scientists and Engineers*. 2013.

[4] P. A. O'Connor and C. J. Cleveland, "U.S. energy transitions 1780-2010," *Energies*, vol. 7, no. 12, pp. 7955–7993, 2014.

[5] P. K. Rohatgi, M. Tabandeh-Khorshid, E. Omrani, M. R. Lovell, and P. L. Menezes, *Tribology for Scientists and Engineers*. 2013.

[6] Lois J. Gschwender, David C. Kramer, Brent K. Lok, Shashi K. Sharma, J. Carl E. Snyder, and Mark L. Sztenderowicz, "10 Liquid Lubricants and Lubrication," *Mod. Tribol. Handb.*, p. 22, 2001.

[7] T. A. Stolarski, "Modern Tribology Handbook," *Tribol. Int.*, vol. 36, no. 7, pp. 559–560, 2003.

[8] J. Fitch, "Don't Ignore Viscosity Index when Selecting a Lubricant," *Trade Journal Publication*, vol. 28956, pp. 1–4, 2012.

[9] D. Johnson, "Tribology Trans- actions," 2018.

[10] G. W. S. A. W. Batchelor, *Engineering Tribology*, vol. 24. ELSEVIER SCIENCE PUBLISHERS B.V. Sara Burgerhartstraat 25 P.O. Box 211,1000 AE Amsterdam, The Netherlands Library, 1993.

[11] M. Nosonovsky, S. V Kailas, and M. R. L. Editors, *Tribology for Scientists and Engineers*. 2013.

[12] P. Studt, "Boundary lubrication: adsorption of oil additives on steel and ceramic surfaces and its influence on friction and wear," *Tribol. Int.*, vol. 22, no. 2, pp. 111–119, 1989.

[13] H. Heinemann, J. G. Speight, and L. R. Rudnick, Eds., *Lubricant Additives: Chemistry and Applications*, Third Edit. Chemical Industries, 2018.

[14] D. A. Johnson, "CHARACTERIZING CHEMICAL CLEANERS USED IN REMOVING VARNISH IN

GAS TURBINE ENGINES," 2018.

[15] T. W. Selby, "The non-newtonian characteristics of lubricating oils," *ASLE Trans.*, vol. 1, no. 1, pp. 68–81, 1958.

[16] M. J. Covitch and K. J. Trickett, "How Polymers Behave as Viscosity Index Improvers in Lubricating Oils," *Adv. Chem. Eng. Sci.*, vol. 05, no. 02, pp. 134–151, 2015.

[17] B. Atherton and U. A. Specialists, "Discovering the root cause of varnish formation," no. April, pp. 1–6, 2007.

[18] L. Ding, R. L. Davidchack, and J. Pan, "A molecular dynamics study of Young's modulus change of semi-crystalline polymers during degradation by chain scissions," *J. Mech. Behav. Biomed. Mater.*, vol. 5, no. 1, pp. 224–230, 2012.

[19] W.-F. Su, *Principles of Polymer Design and Synthesis, Lecture Notes in Chemistry 82.*, vol. 82. 2013.

[20] B. Fayolle, E. Richaud, X. Colin, and J. Verdu, "Review: Degradation-induced embrittlement in semi-crystalline polymers having their amorphous phase in rubbery state," *J. Mater. Sci.*, vol. 43, no. 22, pp. 6999–7012, 2008.

[21] T. R. Crompton, "Chapter 1: Mechanical Properties of Polymers," *Phys. Test. Plast.*, pp. 1–148, 2012.

[22] G. George *et al.*, "Lifetime prediction of biodegradable polymers," *Prog. Polym. Sci.*, vol. 71, pp. 144–189, 2017.

[23] K. Balani, V. Verma, A. Agarwal, and R. Narayan, "Physical, Thermal, and Mechanical Properties of Polymers," *Biosurfaces*, pp. 329–344, 2015.

[24] A. Gleadall, *Mechanical properties of biodegradable polymers for medical applications*. Woodhead Publishing Limited, 2014.

[25] S. P. Lyu *et al.*, "Kinetics and time-temperature equivalence of polymer degradation," *Biomacromolecules*, vol. 8, no. 7, pp. 2301–2310, 2007.

[26] J. C. Fitch and S. Gebarin, "Review of Degradation Mechanisms Leading to Sludge and Varnish in Modern Turbine Oil Formulations," *Oxid. Test. Turbine Oils*, vol. 3, no. 8, pp. 54-54–10, 2009.

[27] A. Yano, S. Watanabe, Y. Miyazaki, M. Tsuchiya, and Y. Yamamoto, "Study on sludge formation during the oxidation process of turbine oils," *Tribol. Trans.*, vol. 47, no. 1, pp. 111–122, 2004.

[28] V. J. Gatto, W. E. Moehle, T. W. Cobb, and E. R. Schneller, "Oxidation Fundamentals and Its Application to Turbine Oil Testing," *Oxid. Test. Turbine Oils*, vol. 3, no. 4, pp. 1-1–20, 2009.

[29] K. Farooq, "Varnish Removal and Control in Turbine Lubrication Systems," pp. 281–287, 2010.

[30] M. Taghvaei and S. M. Jafari, "Application and stability of natural antioxidants in edible

oils in order to substitute synthetic additives," *J. Food Sci. Technol.*, vol. 52, no. 3, pp. 1272–1282, 2015.

[31] N. Truong and N. Corporation, "Today ' s Varnish Control Technologies," 2019. [Online]. Available: https://www.machinerylubrication.com/Articles/Print/1111.

[32] P. Vangla, N. Roy, K. Mendu, and G. M. Latha, "Digital Image Analysis for the Determination of Size and Shape Parameters of Sand Grains," *Golden Jubil. Conf. IGS Bangalore, Geo Innov.*, no. August 2015, pp. 30–31, 2014.

[33] V. J. Gatto, W. E. Moehle, T. W. Cobb, and E. R. Schneller, "Oxidation fundamentals and its application to turbine oil testing," *J. ASTM Int.*, vol. 3, no. 4, p. No-given, 2006.

[34] M. A. Al-Baghdadi, K. K. Resan, and M. Al-Waily, "CFD investigation of the erosion severity in 3D flow elbow during crude Oil contaminated sand transportation," *Eng. Technol. J.*, vol. 35, no. 9, pp. 1–6, 2017.

[35] E. Mobil, "Tech Topic, Coking," vol. 25, no. 2, pp. 1–4, 2004.

[36] E. Rogers and R. C. Arkin, "Determining and solving varnish problems Characterization," *Tribol. Lubr. Technol.*, no. November, 2015.

[37] Energy.gov, "How Gas Turbine Power Plants Work | Department of Energy," pp. 1–4, 2016.

5 Appendix

Table 5-1: Comprehensive test list.

Test type	Date	Varnish mass (mg)	Re Number	Flow	Temp	Concentration	Removal (t) 10% (min)	Removal (t) 90% (min)	Duration (hour)
Commercial	3/9/2018	92.1	361.9	4.5	90	NA	633.83	Not reached	34
	3/29/2018	78.4	359.3	4.5	90	NA	116.17	370.83	11
	4/1/2018	92.8	381.4	4.5	90	NA	274.50	Not reached	22
	4/17/2018	83.9	368.8	4.5	90	Base oil	Not reached	Not reached	35
	5/7/2018	93.8	369.6	4.5	90	NA	1097.83	Not reached	37
Flow	5/29/2018	66.5	368.8	0.5	90	Base oil	Not reached	Not reached	35
	6/5/2018		369.6	0.5	90	20%	75.33	265.17	6
	6/7/2018	82.0	739.2	1.0	90	20%	42.00	176.17	4
	6/11/2018	81.8	1108.8	1.5	90	20%	38.33	167.18	3.5
	6/11/2018	82.3	1478.4	2.0	90	20%	23.50	96.50	3
	8/6/2018	84.3	2956.7	4.0	90	20%	19.67	88.00	2
	8/7/2018	82.5	73.9	0.1	90	20%	147.00	465.50	8
	8/9/2018	79.5	368.8	0.5	90	Base oil	Not reached	Not reached	35
Temperature	8/21/2018	83.7	285.5	0.5	80	20%	61.8	240	5
	8/22/2018	76.4	213.7	0.5	70	20%	60	285	6
	8/27/2018	97.3	154.0	0.5	60	20%	138	505.8	9
	1/17/2019	74.7	370.6	0.5	100	20%	16	128	2.5
Concentration	9/11/2018	87.2	370.6	0.5	90	15%	165.33	435.17	8
	9/12/2018	88.6	371.7	0.5	90	10%	403.50	Not reached	30
	9/20/2018	88.7	371.7	0.5	90	10%	510.50	Not reached	30
	9/26/2018	72.3	372.7	0.5	90	5%	2866.63	Not reached	142
Commercial	8/30/2018	86.1	381.4	0.5	90	NA	Not reached	Not reached	40
	11/2/2018	76.6	369.6	0.5	90	20%	46.50	193.002	4.5
	11/5/2018	82.8	369.6	0.5	90	20%	42.00	176.7	3.5
	11/7/2018	77.5	406.1	0.5	90	NA	Not reached	Not reached	50
	11/26/2018	76.4	382.9	0.5	90	NA	Not reached	Not reached	50
	12/17/2019	84.6	#VALUE!	0.5	90	NA	Not reached	Not reached	51
	12/18/2019	80.1	296.2	0.5	90	NA	40.02	235.8	6
	1/11/2019	89.4	381.4	0.5	90	NA	Not reached	Not reached	50
	1/15/2019	80.5	369.6	0.5	90	20%	24.7	Not reached	4